MicroRNA-21 promotes fibrogenesis in peritoneal dialysis

Melisa Lopez-Anton[1], Mark Lambie[2], Manuel Lopez-Cabrera[3], Claus Peter Schmitt[4], Vicente Ruiz-Carpio[3], Maria Bartosova[4], Betti Schaefer[4], Simon Davies[2], Timothy Stone[1], Robert Jenkins[1], Philip R. Taylor[1], Nicholas Topley[1], Timothy Bowen[1], and Donald Fraser[1*]

From Wales Kidney Research Unit, Division of Infection and Immunity, School of Medicine, College of Biomedical and Life Sciences, Cardiff University, Cardiff, United Kingdom, CF14 4XN

[1] Cardiff University, Cardiff, United Kingdom

[2] Keele University, Keele, United Kingdom

[3] Centro de Biología Molecular Severo Ochoa, CSIC, Madrid, Spain

[4] University of Heidelberg, Heidelberg, Germany

*Address Correspondence to: Donald Fraser PhD FRCP, Wales Kidney Research Unit, Cardiff University, Heath Park Campus, Cardiff, UK, CF14 4XN; Telephone +44(0)2920748449; Email: fraserdj@cf.ac.uk

Running Title: miR-21 in peritoneal dialysis

This work was supported by Marie Curie Innovative Training Network 287813, "European Training and Research in Peritoneal Dialysis"

Disclosures: None Declared

Abstract

Peritoneal dialysis (PD) is a life-saving form of renal replacement therapy for those with End Stage Kidney Disease. Mesothelial Cells (MC) line the peritoneal cavity and help define peritoneal response to treatment-associated injury, a major reason for treatment failure. MicroRNAs (miRNAs) are important regulators but their roles in peritoneal fibrosis are largely unknown.

In this study microRNA-21 (miR-21) was one of the most abundant miRNAs in primary MCs, and was up regulated by the profibrotic cytokine TGF-β1 and in PD effluent-derived MCs exhibiting mesenchymal phenotypic change. Increased miR-21 was found in peritoneal membrane biopsies from PD patients compared to healthy controls (PD biocompatible, 5.86x, p=0.0001; PD conventional, 7.09x, p<0.0001, n=11 per group). In PD effluent from a cohort of 230 patients, miR-21 was higher in those receiving the therapy long-term compared to new starters (n=230, miR-21 3.26x, p=0.001) and associated with Icodextrin usage *R*=0.52, (0.20, 0.84), peritonitis count *R*=0.16, (0.03, 0.29) and dialysate cytokines. MiR-21 down-regulated Programmed Cell Death 4 (PDCD4) and PDCD4 protein was decreased in peritoneal membrane biopsies from PD patients compared to healthy controls. New miR-21 targets were identified that may be important during peritoneal dialysis fibrogenesis. These data identify miR-21 as an important effector of fibrosis in the peritoneal membrane, and a promising biomarker in the dialysis effluent for membrane change in patients receiving PD.

Introduction

End stage kidney disease means that 650,000 people in The United States depend on renal replacement therapy to keep them alive, a number increasing by 5-8% per year. Dialysis treatment accounts for 1-2% of national healthcare budgets, and may be provided by hemodialysis, in which the blood is purified across an artificial membrane, or by peritoneal dialysis (PD). In PD, exchange between the blood and the dialysate instilled in the patient's own peritoneal cavity occurs across the peritoneal membrane. Thus, PD leads to constant exposure of the peritoneal membrane to bioincompatible PD solutions and a basal inflammatory state, resulting in membrane damage that may progress to treatment failure[1]. Alterations in mesothelial cell (MC) phenotype, including acquisition of a mesenchymal phenotype and mesothelial cell loss, are an important determinant of these sequelae[2], leading to increased synthesis of extracellular matrix components and release of pro-inflammatory and pro-angiogenic factors[3]. MCs are also detectable in the spent dialysate, and acquire a progressively non-epithelioid phenotype with longer duration dialysis[4]. Cells in the deeper layers of the peritoneal tissue, including the stromal fibroblast population, may also make key contributions to fibrogenesis[5].

Induction of *in vitro* and *in vivo* mesenchymal trans-differentiation by TGF-β1 has been well documented in the peritoneal membrane and other tissues and organs[3, 6, 7]. TGF-β1 overexpression induces structural and functional membrane alterations in rat and mouse peritoneum[7, 8] and intra-peritoneal inhibition of TGF-β1 preserves peritoneal morphology and function in this model[3]. TGF-β1-driven phenotypic change in primary

MCs is therefore a valuable model to study mechanisms of peritoneal fibrosis progression associated with PD therapy[9].

MicroRNAs (miRNAs) are short, non-coding RNAs that regulate gene expression at the post-transcriptional level. One miRNA may regulate the expression of hundreds of target mRNAs, profoundly affecting cell phenotype and function. Alterations in miRNA expression have been described in a wide range of *in vitro* and *in vivo* models[10]. Studies on miRNA expression in different model systems and body fluids have emphasized their potential as therapeutic targets and disease biomarkers[11-14]. Mesothelial cell miRNA expression, function, and role of miRNAs in peritoneal fibrosis are largely unknown, and recent studies have begun to address this (reviewed in[15]). Quantification of 7 miRNAs in PDE-derived cells from 28 prevalent PD patients found correlation with peritoneal transport characteristics[16]. Enforced expression of miR-29b inhibited peritoneal fibrosis in a mouse model of daily intraperitoneal PD fluid infusion[2]. MiR-30a was down regulated in a rat PD infusion model, and decreased in peritoneal membrane from 10 established PD patients[17]. In this last study, miR-30a targeted Snail, a key regulator of mesothelial to mesenchymal transition (MMT) via down-regulation of adherens (E-cadherin) and tight junctions (Claudin-1, Occludin and ZO-1)[18, 19]. MiR-589 was down-regulated in 6 PD patients treated for more than 6 months[20] and miR-200c was down-regulated in PDE-derived cells from 16 patients undergoing PD for more than 6 months[21]. Collectively, these studies are suggestive that miRNAs are important regulators of MC phenotype and fibrogenesis in PD patients. Measurement of miRNAs in PDE may, therefore, be valuable in predicting the clinical course. However, this previous research has largely taken a literature-based

candidate miRNA approach, and drawn conclusions from analyses of small numbers of patient-derived samples.

In this study, miRNAs were studied in mesothelial cells cultured *in vitro* and *ex vivo* from peritoneal dialysis patients, and linked to measurements conducted in the peritoneal dialysis effluent and the peritoneal membrane itself, to provide definitive identification of microRNAs expressed by MC's and changes occurring as a consequence of peritoneal dialysis, and to link these to likely microRNA functions. MC miRNA profiles and responses to TGF-β1 were characterized *in vitro*, and increased miR-21 was demonstrated in MCs incubated with TGF-β1, and in separate experiments in MCs exhibiting a mesenchymal phenotype derived from PDE. In a study of 44 peritoneal membrane biopsies, increased miR-21 was found in peritoneal membrane from PD patients compared with healthy and uremic controls. In PDE from a cohort of 230 patients taken from The Global Fluid Study, miR-21 associated with clinical parameters indicative of membrane change and treatment failure. Analysis of miRNA targets identified miR-21 regulation of tumor suppressor programmed cell death 4 (*PDCD4*) in MCs and in peritoneal membrane biopsies from PD patients. Finally, four previously unreported miR-21 targets were identified, linked to the mesothelial to mesenchymal process occurring as a consequence of PD treatment.

Materials and Methods

Cell culture, TGF-β1 treatment and Cell Transfection

Appropriate ethical approval was in place for all experiments involving specimens derived from patients, and all patients gave informed consent for use of their specimens for research purposes. Human peritoneal mesothelial cells (HPMCs) were obtained from enzymatically degraded specimens of human omentum as previously reported[22]. In brief, specimens of omentum from patients undergoing abdominal surgery were washed in PBS before incubation with 0.125% (w/v) trypsin, 0.01% (w/v) EDTA and 0.1% (w/v) glucose for 20 mins at 37^{o}C with continuous rotation. After incubation the suspension was centrifuged at 50x g for 5 mins at 4^{o}C. The cell pellet was washed once in culture medium, then resuspended in culture medium and seeded in tissue culture flasks. For *ex vivo* analysis, mesothelial cells derived from PD patients' effluents were cultured and analyzed as described[4]. In brief, Human mesothelial cells from peritoneal dialysis effluent were obtained by centrifugation and passaged in culture two times at 10 to 15 day intervals. Morphologic features of cells were compared and remained stable through passage. Mesothelial cells were characterized as of epithelial or fibroblast-like character as previously reported[4].

For microRNA gain- and loss-of function experiments, mirVana miRNA mimic and mirVana miRNA inhibitors were used at concentrations of 5 pM, 10 pM and 20 pM for target mRNA measurements 48 h after transfection. 5 pM of *mir*Vana miRNA mimic were used for protein quantification 72 h after transfection.

Peritoneal Membrane Study

FFPE peritoneal membrane samples from 44 pediatric patients (1.83-19.16 years old) included in the International Pediatric PD Biopsy Study were used in this analysis (www.clinicaltrials.gov, NCT01893710). Patients were matched for age, sex, PD

duration and submesothelial thickness. Patients with previous peritonitis, systemic diseases and abdominal surgery other than Tenckhoff catheter insertion, revision or kidney transplantation were excluded. Comprehensive individual clinical data were collected and assessed before analysis to exclude disparity regarding disease susceptibility or comorbidity. Approval was obtained from local ethics committees, and written informed consent obtained from patient and parents. FFPE samples were cresyl violet stained and the mesothelial and submesothelial compact zone were manually micro dissected from a total of 40 µm section using a Leica RM 2165 rotary sliding microtome and a Leica S8 APO stereo microscope.

PD Effluent Study

The Global Fluid Study is an international, multicenter, prospective, observational cohort study of 959 patients[24]. Samples from a single center were used for microRNA analysis, to exclude center effects, and the first sample collected from each patient was analyzed. Dialysate cytokine levels had been measured previously by electrochemiluminescence[24]. 4-hour dwell dialysate samples were stored at -80°C and thawed on ice. 600 µl aliquots were centrifuged at 12,000g at 4°C for 20 min prior RNA extraction. Extreme outliers (3) were re-tested and then excluded, as the results from these samples showed high variance, consistent with sample degradation prior to analysis.

RNA isolation

For RT-qPCR analysis, miRNA and mRNA arrays HPMCs were lysed in TRI reagent (Ambion, Life Technologies), and RNA was extracted as recommended by the

manufacturer. RNA from PDE was isolated from 500 µl of fluid using the mirVana PARIS Kit (Ambion, Life Technologies). To monitor extraction efficacy, 0.5 pmol of cel-miR-39 (Life Technologies, MC10956) was spiked-in to all PDE samples after addition of 2x denaturing solution. Formalin-fixed, paraffin-embedded (FFPE) samples were processed immediately after sectioning using RecoverAll™ total nucleic acid isolation kit (Ambion, Life Technologies) according to the manufacturer's recommendations. 1 µg of MS2 RNA carrier (Roche) was added to biopsy extractions, to improve RNA recovery.

Reverse Transcriptase-quantitative Polymerase Chain Reaction (RT-qPCR) Analysis

cDNA was synthesized from 2 µg of total RNA using the High Capacity cDNA reverse transcription kit (Life Technologies). Alternatively, 10 ng of total RNA were used for cellular miRNAs. For PDE and FFPE samples, constant volumes of RNA were used. RT-qPCR was carried out in a ViiA™ 7 Real-Time PCR System (Applied Biosystems) using Power SYBR Green PCR master mix (Applied Biosystems). The primers used are shown in Table 1. Taqman Universal Master Mix II (Applied Biosystems) and specific primers for miR-21 and miR-191 (Applied Biosystems) were used for miRNA analysis[25]. mRNA and miRNA expression were normalized to GAPDH and miR-191 respectively. The relative changes in gene expression were analyzed by the $2^{-\Delta\Delta Ct}$ method[26].

miRNA and mRNA microarrays

Microarray assays were performed on HPMCs derived from four independent donors. miRNA expression was measured in control samples and after 1 ng/ml of TGF-β1 treatment for 48 h[3, 27-30]. Confirmed in all samples by analysis of eight molecular

markers chosen as indicators of epithelial (E-Cadherin, ZO-1, Claudin and Occludin) and mesenchymal (Fibronectin, Collagen I, Snail and α-SMA) phenotype (unpublished data and[3, 27-30]). A total of 1 µg in a volume of ≤2 µl of total RNA from each sample was subsequently used for *Toray* microarray analysis, performed by Central Biotechnology Services at Cardiff University as described previously[31]. For ex vivo mRNA microarray analysis patient derived MCs samples were classified as: E phenotype (9 samples) and NE phenotype (8 samples)[30]. Four omentum-derived MC samples were taken as controls. Label dye-swap design was used in these experiments using the Quick Amp Labeling Kit, two-color (Agilent Technologies, Santa Clara, California, USA). mRNA microarray analysis was carried out using the Whole Human Genome Microarrays Kit 4x44 K (Agilent Technologies) according to the manufacturer's instructions: 825 ng of cRNA (Cy3-cRNA and Cy5-cRNA) were incubated with blocking agent and fragmentation buffer, 30 minutes, 60°C. Hybridization was performed in hybridization buffer at 65°C for 17 hours in darkness and stirring at 10 rpm. Subsequently, slides were introduced in different saline buffer stringencies, stabilization solution and dried as indicated by Agilent Technologies. Arrays were scanned on the Agilent Technologies G2505B Micro Array Scanner at 5 nm resolution.

Immunoblotting

Whole cell protein samples were collected using RIPA Lysis Buffer (Santa Cruz Biotechnology, sc-24948) and protein concentrations were determined using BioRad Protein Assay (BioRad, 5000001). 15 µg of protein in 3x Reducing Loading Buffer were heated at 95°C for five minutes, ice-cooled, separated by 7.5% SDS-PAGE and transferred onto nitrocellulose membranes which were subsequently blocked using 5%

BSA with 0.1% Tween 20 for 1 hour. Primary and secondary antibodies were PDCD4 (1:1000; #9535 D29C6; Cell Signaling Technology), GAPDH (1:2000; ab9485; Abcam), goat anti-rabbit IgG-HRP (1:10000; sc-2004; Santa Cruz Biotechnology) and goat anti-mouse IgG-HRP (1:10000; sc-2005; Santa Cruz Biotechnology) incubated in 0.1% BSA with 0.1% Tween-20 overnight. Immunoblots were developed using WesternBright ECL Spray (Advansta, K-12049-D50), images were captured via C-DiGit Chemiluminescent Western Blot Scanner and densitometry analysis was conducted using Image Studio Version 5.2 Software.

Immunohistochemical staining

Immunohistochemical staining of peritoneal membrane study samples was performed on 5 μm sections mounted on glass slides as previously described[32]. After deparaffinization and rehydration the sections were incubated in 3% hydrogen peroxide. Heat-induced antigen retrieval was performed in a microwave oven, using 0.005 M citrate buffer (pH 6). Polyclonal rabbit anti p-SMAD2/3 (Santa Cruz, California, sc-11769) was incubated for 1 h at room temperature (1:100). Incubation with biotinylated secondary reagents (Vector) for 30 min was followed addition of ABC reagent (Vector) and detection using 3′ 3′ Diaminobenzidine (DAB, Sigma, Taufkirchen, Germany) with haematoloxylin counterstain.

Aperio Analysis

Immunohistochemical images were captured and evaluated using Aperio Precision Image Analysis Software (USA). The Positive Pixel Count Algorithm (version 9) output was used to calculate total p-SMAD2/3 staining. Input algorithm parameters are

specific color ranges in the HSI colorspace (Hue value 0.1; Hue width 0.5) and intensity ranges to differentiate between weak, medium, strong and negative staining. Intensity thresholds (upper/lower limit): weak 220/175, medium (175/100), strong (100/0) and negative (255/220). Thresholds were optimized and validated specifically for p-SMAD2/3. Positivity was calculated using numbers of negative pixels (N_n) and total pixels (N_{total}) using the formula: (N_{total}-N_n)/(N_{total}).

Statistical Analysis

Differences between two individual experimental groups of normally distributed values were compared by two-tailed *t* test, for multiple comparisons, ANOVA followed by post hoc Holm-Sidak's test was used. For clinical data, Pearson's correlations were used for normally distributed variables, transformed as necessary, and Spearman's for other variables. Multivariable linear regression with backwards-stepwise variable selection was performed for natural log transformed miR-21 variables, and to avoid problems with suppressor effects, dialysate cytokine values were entered as a block.

miRNA Array data were analyzed using GenePix Pro software, spot data were considered valid probe hybridization when signal intensity was greater than the mean intensity of the background signal plus 2 standard deviations. A normalization step for each specific miRNA adjusted median value was subsequently performed. The relative miRNA expression levels were determined by comparing the mean signal intensity of the real hybridized spots with their average value across the microarray experiment. To reliably compare data from multiple chips, a quantile-normalization was applied to the values. These microRNA profiling datasets can be found in GEO (GSE79006).

mRNA array data processing and normalization was performed using the Babelomics software[30,33]. Fluorescence raw signal from each probe was corrected with the subtraction of local background and normalized with the loess method (within arrays) or the quantile method (between arrays). Fold change for a gene was determined as a quotient between normalized data from samples under study. Statistics for differential expression was obtained with Limma One Class or Limma Two Class test and corrected for multiple-test with FDR (False Discovery Rate; Benjamini & Hochberg). Genes with fold change ≤0.5, and FDR≤0.01, were considered repressed. mRNA array changes displayed here indicate gene rather than transcript variant level. mRNA array results presented in this article can be found in GEO (GSE92455)[30].

Results

Mesothelial miRNA profile is altered by TGF-β1

Before profiling overall mesothelial miRNA expression a characterization of responses to TGF-β1 was performed using primary cultures of mesothelial cells with replicate experiments using cells from different omental donors (Supplemental Figure 1 and 2). These results demonstrated that in primary HPMCs from multiple donors, 1 ng/ml of TGF-β1 induced changes consistent with an MMT process after 48 h. Global miRNA expression was then quantified by hybridization array. Four independent biological replicates from different donors displayed high consistency (Supplemental Figure 3). A total of 699 miRNAs were detected in at least three samples and were included in subsequent analysis. 95 of 699 miRNAs were differentially regulated by TGF-β1. MiR-

21 and miR-31 were highly expressed by HPMCs and induced by TGF-β1 treatment (Figure 1A). MiR-29b, previously shown to limit fibrosis when over-expressed in a mouse PD fluid infusion model[2], was detected at high signal intensity, but no significant change was observed in response to TGF-β1 (fold change: 0.95x, p=0.61). Additional miRNAs previously associated with peritoneal membrane transport change and fibrosis were detected at low signal intensity in this profile and did not change significantly in response to TGF-β1 (including miRs -15a, -17, -30, -192, -200c, -377, -589).

Up-regulation of miR-21 and miR-31 in primary HPMCs was validated using miRNA-specific Taqman RT-qPCR assays (fold change: miR-21, 1.8x, p=0.012; miR-31, 1.7 x, p=0.004 (Figure 1B and Supplemental Figure 4A). Subsequently, miR-21 and miR-31 expression was evaluated in PDE-derived HPMCs cultured *ex vivo*, divided as previously described[4] into those exhibiting phenotypic changes consistent with early (E: epithelial phenotype) or late (NE: non-epithelial phenotype) mesothelial to mesenchymal transition. MiR-21 exhibited a stepwise increase in expression through cells of progressively more mesenchymal phenotype (Control, incubated with TGF-β1, effluent-derived epithelioid, effluent-derived non-epithelioid) (Figure 1C). Elevation of miR-31 in this model was also confirmed (Supplemental Figure 4B).

<u>TGF-β1 signaling is activated, and miR-21 expression is increased, in PD patient peritoneal membrane biopsies</u>

TGF-β1 signaling, miR-21 and miR-31 expression were analyzed in the mesothelial and sub-mesothelial cell layers of patients undergoing PD. In order to evaluate the effects

of the therapy, distinct from associated vascular pathology or other comorbidity that may be present in biopsies from adult patients, samples from the International Pediatric Membrane Biopsy Registry were studied. Children undergoing PD with conventional and with biocompatible fluids were examined, and compared with uremic and non-uremic controls (n=11 per group, mean age at biopsy: PD conventional 9.1 years, PD biocompatible 8.9 years, control uremic 9.6 years, control non-uremic 8.0 years; mean duration of PD: PD conventional 30 months, PD biocompatible 31 months). α-SMA staining was used as an indictor of fibrogenesis in these samples (Supplemental Figure 5) while SMAD2 and SMAD3 phosphorylation were determined as a measure of TGF-β1 activity. Phospho-SMAD2/3 staining of formalin-fixed paraffin embedded (FFPE) samples was measured using Aperio Precision Image Analysis Software and a count algorithm for positive pixel detection together with positive and negative controls (Figure 2A-C). The mesothelial and sub-mesothelial compact zone of PD patients displayed enhanced TGF-β1 pathway activation compared with controls (Figure 2A-C). Enhanced p-SMAD2/3 signal was observed in the mesothelium of PD patients under conventional PD fluid treatment compared with controls (Figure 2C). MiRNA analysis of manually micro-dissected FFPE samples also showed an increase in miR-21 expression in the mesothelium of PD patients (Figure 2D). Significant up-regulation of miR-21 was evident following PD treatment when all the groups were compared with controls (Figure 2D). Due to a high variability between samples in the control group, no difference was seen between healthy controls and PD patients in miR-31 peritoneal membrane expression. However, a trend of up-regulation in miR-31 expression was observed between uraemic controls and PD patients (Supplemental Figure 4C).

Previous studies have identified direct targeting by miR-21 of programmed cell death protein 4 (*PDCD4*)[34-36], and sequence analysis demonstrated a conserved target site for miR-21 (Supplemental Figure 6F). To confirm that this was relevant in the peritoneal membrane *in vivo*, expression of PDCD4 was examined in samples from the pediatric peritoneal membrane biopsy registry. Peritoneal membrane biopsies from PD patients showed a significant down-regulation in PDCD4 expression in the mesothelial and sub-mesothelial compact zones when compared with controls (Figure 2E-G). Taken together, these data are in line with repression of PDCD4 by miR-21 contributing to MMT and promotion of fibrosis in the peritoneal membrane.

MiR-21 expression in PD Effluent correlates with clinically important parameters

To assess the potential of miR-21 as a biomarker, miRNA expression was analyzed in patient PDE samples. Initial experiments demonstrated stability of miRNA signal for at least 8h following sample collection (data not shown). Subsequently, samples of effluent dialysate following a 4-hour standardized dwell in a cohort of 230 patients recruited to The Global Fluid Study[24] in a single center were analyzed. Supplemental Table 1 displays baseline clinical characteristics of the patients. When measured in effluent of prevalent PD patients, miR-21 and miR-31 expression levels were strongly increased in comparison with incident cases (fold change: miR-21 3.26x, p=0.001; miR-31, 1.84 x, p=0.0007) (Figure 3A and Supplemental Figure 7).

To investigate the relationship between miR-21, miR-31 and parameters associated with poor PD outcome we performed an exploratory correlation analysis in which miR-21 better correlated with parameters associated with an inflammatory condition

(Supplemental Table 2). In order to understand the relevance of these variables for the described miR-21 up-regulation we performed a multivariable linear regression with backwards-stepwise variable selection for all parameters included in Supplemental Table 2 and miR-21 or miR-31 (Table 2 and Supplemental Table 3). Consequently, stepwise variable selection determined a group of tighter risk factors that associated with miR-21 in predicting PD outcome. miR-21 associated with dialysate Icodextrin usage *R*=0.52, (95% confidence intervals 0.20, 0.84), peritonitis count *R*=0.16, (0.03, 0.29), miR-31 *R*=0.52 (0.15, 0.90) and dialysate cytokines (Table 2). miR-31 associated with biocompatible solution use *R*=0.18 (-0.04, 0.40), use of CAPD vs. APD *R*=0.14 (0.02, 0.25), miR-21 *R*=0.087 (0.038, 0.136), peritonitis count *R*=0.052 (0.006, 0.098), plasma albumin *R*=0.0096 (-0.001, 0.020) and urine volume *R*=-0.0001 (-0.00017, -0.00003 (Supplemental Table 3). Recent work shows that IL-6 and IFN-γ cooperate to shift acute peritoneal inflammation into a more chronic pro-fibrotic state following recurrent inflammatory episodes[37]. IL-6 concentration in PD effluent is the most significant known predictor of peritoneal small solute transport rate (PSTR)[24]. While IFN-γ shows a strong correlation with localized intraperitoneal inflammatory networks[24]. In the current study, association between miR-21 and IL-6 was of borderline significance on multivariable linear regression (*R*=0.28, 95% CI -0.02, 0.58) while dialysate IFN-γ was highly significant (*R*=-0.77, 95% CI -1.21, -0.33) when adjusted for dialysate IL-6. Here, we used values from the range of dialysate IFN-γ stratified by the 25th, 50th and 75th centiles for dialysate IL-6 and showed strong prediction of miR-21 expression (Figure 3B).

Identification of miR-21 targets that may contribute to MMT during PD therapy

PDCD4 is an important effector of miR-21-induced fibrotic change in other contexts, and here we have found PDCD4 to be down regulated in the peritoneal membrane of patients treated with PD (Figure 2E-G). However, microRNAs typically have several hundred targets and may be predicted to control changes in cell phenotype *via* broad actions across many targets. To have a more complete understanding of how miR-21 up-regulation may lead to MMT and fibrosis in the peritoneal membrane, predicted miR-21 targets were evaluated in an Affymetrix array dataset comprising profiles of control, early- and late-MMT, using patient-derived effluent mesothelial cells cultured *ex vivo* as previously described[4]. Overall, 774 genes were identified as down regulated in the MMT process, including 274 transcripts identified as down-regulated specifically in early MMT and 298 transcripts in late MMT (Figure 4A). Independent miR-21 target prediction was undertaken using four different algorithms, and results subsequently combined, comprising Diana[38, 39], miRDB[40, 41], miRanda[42, 43] and TargetScan[44, 45] (Figure 4B). Single miR-21 algorithm predictions were inter-crossed to identify targets that were predicted by three or more algorithms (Figure 4B). These predicted miR-21 targets were further inter-crossed with the genes identified as down regulated in MMT (Figure 4C). Five miR-21 predicted targets were identified to be differentially down regulated during early-MMT, two in the late-MMT course and ten when the whole-MMT was evaluated (Figure 4C). These included -early MMT- Natriuretic Peptide B (*NPPB*), *PDZD2*, S100 calcium-binding protein A10 (*S100A10*), SAM And SH3 Domain Containing 1 (*SASH1*) and Metalloproteinase inhibitor 3 (*TIMP3*); -late MMT- *PDZD2* and *SASH1*; and -whole MMT- Absent In Melanoma 1-Like (*AIM1L*), CASK Interacting Protein 1 (*CASKIN1*), Dual Specificity Phosphatase 8 (*DUSP8*), Fibroblast Growth Factor

18 (*FGF-18*), Matrilin 2 (*MATN2*), Neural EGFL Like 2 (*NELL2*), *PDZD2*, (Ras Homolog Family Member B (*RHOB*), *SASH1* and Sprouty RTK Signaling Antagonist 1 (*SPRY1*).

Evaluation of miR-21 targets in HPMCs under MMT conditions

The above analysis provided 14 predicted miR-21 targets identified as down regulated in *ex-vivo* cultured mesothelial cells exhibiting MMT. These 14 genes were subsequently examined by RTqPCR in mesothelial cells exhibiting progressively more mesenchymal phenotype (control, incubated with TGF-β1, effluent-derived epithelioid, effluent-derived non-epithelioid). 11 of 14 genes demonstrated a pattern of expression consistent with miR-21 regulation in this model (Figure 5 and Supplemental Figure 8). *mirVana* miR-21 mimic and inhibitor delivery in HPMCs was used to evaluate these 11 predicted targets. Five targets showed significant down regulation by miR-21 mimic and up regulation by inhibitor, namely *PDZD2*, *S100A10*, *FGF-18*, *MATN2* and *PDCD4* (Figure 6). CASKIN1, NELL2 and DUSP8 were up regulated by miR-21 inhibitor but did not show significant change in response to enforced expression of miR-21, and SASH1 and AIM1L expression was not affected by enforced expression/repression of miR-21 (Supplemental Figure 9).

Analysis of 3'UTR target site types and conservation for the identified targets *PDZD2, S100A10, FGF-18*, *MATN2* and miR-21 across different animal species is shown in Supplemental Figure 6. *PDZD2* 3'UTR was found to contain two different seed region consensus sites, while the remainder of the targets identified each had a single miR-21 predicted binding site in the UTR (Supplemental Figure 9). Sites identified were highly

conserved and energetically favorable (8mer or 7mer-m8 sites, [46]) in keeping with direct regulation of these targets.

Discussion

PD is an effective form of renal replacement therapy, but is often limited by deterioration in the structural and functional characteristics of the peritoneal membrane. New biomarkers are needed, to help individualize therapy in PD, to serve as appropriate surrogates in clinical trials, and to guide development of innovations in the therapy. miRNAs show promise as biomarkers in patients with kidney disease[6, 47] but there has been limited study to date in PD patients. Our data show that miR-21 expression is increased in several well-established models associated with structural and functional alterations of the peritoneal membrane during peritoneal dialysis. Moreover, we showed that miRNAs can be measured in the peritoneal dialysis effluent from PD patients, where miR-21 correlates with clinical parameters indicating poor outcome on PD.

The peritoneal membrane has a complex structure, and includes cells of multiple lineages. The mesothelial cell layer forms the interface between dialysate and membrane, and plays an important role in determining changes associated with PD therapy failure[9]. TGF-β1 plays a pivotal role in PD treatment-driven membrane alterations[3] and here we have defined a pattern of microRNA changes occurring in primary human mesothelial cells in response to TGF-β1. These data showed abundant

expression of miR-21 in mesothelial cells, and increased expression when cells were incubated with TGF-β1. Previous studies have characterized the phenotype of mesothelial cells isolated from PDE from patients and demonstrated that a progressive loss of epithelial morphology is accompanied by a decrease of Cytokeratins and E-cadherin expression as well as an induction of the transcriptional repressor Snail[4]. Further experiments found increased miR-21 in PDE-derived mesothelial cells with these mesenchymal characteristics, linking miR-21 to mesothelial cell characteristics previously shown to define an adverse response to PD[4].

Subsequently, miR-21 expression was examined in peritoneal membrane biopsies. Fibro-proliferative changes have been delineated in the peritoneal membrane of PD patients, together with more minor changes in uremic (pre-dialysis) patients[48]. Peritoneal vascular changes are also frequently evident in adult patients, which may make it difficult to separate therapy-induced alterations from those related to the propensity of individuals with CKD to accelerated cardiovascular disease. At the time of PD onset, the pediatric peritoneal tissue is devoid of vascular alterations and tissue aging. In order to determine the "pure" effects of the therapy, pediatric biopsy samples were examined, from the International Pediatric Peritoneal Biopsy Registry. TGF-β1 signaling was clearly evident in biopsies from PD patients compared to controls, and was associated with increased miR-21 and decreased PDCD4 in the mesothelial and sub-mesothelial zones. Given recent fate mapping studies, which have delineated an important contribution of sub-mesothelial fibroblasts to peritoneal fibrosis in mouse models[5], understanding the potential role of miRNAs including miR-

21 in sub-mesothelial fibroblast phenotype may also be an important future area of study.

Inflammatory markers, most notably Il-6, may be measured in the dialysis effluent as an indirect measure of intraperitoneal inflammation[49], although a biomarker for the extent of peritoneal fibrosis is still lacking. Multivariable linear regression with backwards-stepwise variable selection was performed, to understand associations of miR-21 expression with clinical characteristics and measures of intraperitoneal inflammation. Of note, miR-21 correlated with Icodextrin usage, which has been previously associated with multiple indicators of local inflammation[24, 50]. The relationship between intra-peritoneal inflammation and membrane function has also been recently investigated in PD patients[24, 51]. In the current study, we also found miR-21 association with peritonitis count and dialysate IFN-γ, IL-6, TNF-α and IL-1β, suggesting a primary response to local factors and inflammatory stimuli. IFN-γ[52], TNF-α and IL-1β[53] induce IL-6 secretion by mesothelial cells, the major producers of IL-6 within the peritoneal cavity[53, 54]. IL-6, in turn, is also an important inducer of miR-21 in multiple myeloma, mammary epithelium, hepatocellular carcinoma (HCC), oral squamous cell carcinoma and keratinocytes *via* STAT signaling[55-59], providing a potential mechanistic basis for the association of pro-inflammatory cytokines with miR-21 expression in the context of peritoneal dialysis.

Here, we identified miR-21 mediated repression of PDCD4 in mesothelial cells. PDCD4 down-regulation triggers an increase in SNAIL protein and a consequent decrease in E-cadherin expression, which in turn stimulates β-catenin/TCF dependent transcription[34-

[36]. Thus, miR-21 down-regulation of PDCD4 in HPMCs may not only contribute to the detachment of inter-mesothelial adhesions but also to the acquisition of a new molecular program, dictating a distinct expression regulation characteristic of an MMT process. In addition, we identified four new miR-21 targets that may be important in the context of PD therapy associated fibrogenesis, *PDZD2*, *S100A10*, *FGF-18* and *MATN2*. Previous literature has linked a reduction of expression of these genes with fibrosis in different contexts. In brief, mice with conditional deletion of FGF-18 in the lung displayed thicker interstitial mesenchymal compartments, embedded capillaries and reduced cell proliferation[60] while FGF-18 over-expression in lung decreased extracellular matrix and connective tissue components including matrilin-2[61]. Between the multiple functions attributed to S100A10 probably the most physiologically remarkable is its extracellular function as a plasminogen receptor, mediating its activation by plasminogen activators, stimulating plasminogen conversion to wide protease plasmin and promoting fibrinolysis[62]. Indeed, S100A10-null mice, although viable, showed impaired fibrinolysis and increased tissue fibrin deposition including in lungs, liver, spleen and kidney compared to wild-type mice litter mates[62]. Matrilin-2 binds collagen I and non-collagenous proteins[63] contributing to extracellular matrix supra-molecular organization. Matrilin-2 knock-down induced serious defects in skin wound healing[64]. Additionally, Ichikawa *et al.* 2008 showed that matrilin-2 reduction in human keratinocyte cells induced cell migration into a wound[64]. *In vitro* treatment with recombinant sPDZD2 induces p53 up-regulation in human prostate cancer (DU-145), breast adenocarcinoma (MCF-7) and liver cancer (Hep-G2) cell lines[65], and such altered p53 activity may inhibit EMT[66]. Importantly though, PDZD2 is expressed in the

nucleus and also secreted following cleavage[67] suggesting a potentially complex role in these processes.

In PD patients, continuous dialysis fluid exchanges allow easy access to monitor peritoneal miRNA expression. Previous studies have demonstrated that Il-6 and IFN-γ are strong predictors of MC damage in PD patients, and are mechanistically linked to peritoneal fibrosis following infection[37]. Nevertheless, no biomarker or combination of biomarkers yet allows prediction of outcome for the single patient or individualized therapy. In this study, microRNAs were found to be stable and readily detected in the peritoneal dialysis effluent, emphasizing their potential as a class of biomarker in this context. MiR-21 was found to be up regulated in mesothelial cells undergoing MMT, and in peritoneal membrane undergoing fibrosis in the context of PD. miR-21 was further found to be stable in dialysis effluent, and PD effluent levels to correlate with different clinically important parameters themselves linked to membrane change in this patient group. These data identify miR-21 as a promising biomarker to monitor the peritoneal membrane of patients undergoing PD therapy.

Acknowledgements

We are grateful to the staff of National Center for Tumor Diseases (NCT, Heidelberg, Germany) and Institute of Pathology (Heidelberg University Hospital) for technical assistance.

References

[1] Aroeira LS, Aguilera A, Sánchez-Tomero JA, Bajo MA, del Peso G, Jiménez-Heffernan JA, Selgas R, López-Cabrera M: Epithelial to mesenchymal transition and peritoneal membrane failure in peritoneal dialysis patients: pathologic significance and potential therapeutic interventions. J Am Soc Nephrol 2007, 18:2004-13.

[2] Yu JW, Duan WJ, Huang XR, Meng XM, Yu XQ, Lan HY: MicroRNA-29b inhibits peritoneal fibrosis in a mouse model of peritoneal dialysis. Lab Invest 2014, 94:978-90.

[3] Loureiro J, Aguilera A, Selgas R, Sandoval P, Albar-Vizcaíno P, Pérez-Lozano ML, Ruiz-Carpio V, Majano PL, Lamas S, Rodríguez-Pascual F, Borras-Cuesta F, Dotor J, López-Cabrera M: Blocking TGF-β1 protects the peritoneal membrane from dialysate-induced damage. J Am Soc Nephrol 2011, 22:1682-95.

[4] Yáñez-Mó M, Lara-Pezzi E, Selgas R, Ramírez-Huesca M, Domínguez-Jiménez C, Jiménez-Heffernan JA, Aguilera A, Sánchez-Tomero JA, Bajo MA, Alvarez V, Castro MA, del Peso G, Cirujeda A, Gamallo C, Sánchez-Madrid F, López-Cabrera M: Peritoneal dialysis and epithelial-to-mesenchymal transition of mesothelial cells. N Engl J Med 2003, 348:403-13.

[5] Chen YT, Chang YT, Pan SY, Chou YH, Chang FC, Yeh PY, Liu YH, Chiang WC, Chen YM, Wu KD, Tsai TJ, Duffield JS, Lin SL: Lineage tracing reveals distinctive fates for mesothelial cells and submesothelial fibroblasts during peritoneal injury. J Am Soc Nephrol 2014, 25:2847-58.

[6] Bowen T, Jenkins RH, Fraser DJ: MicroRNAs, transforming growth factor beta-1, and tissue fibrosis. J Pathol 2013, 229:274-85.

[7] Margetts PJ, Bonniaud P, Liu L, Hoff CM, Holmes CJ, West-Mays JA, Kelly MM: Transient overexpression of TGF-{beta}1 induces epithelial mesenchymal transition in the rodent peritoneum. J Am Soc Nephrol 2005, 16:425-36.

[8] Margetts PJ, Kolb M, Galt T, Hoff CM, Shockley TR, Gauldie J: Gene transfer of transforming growth factor-beta1 to the rat peritoneum: effects on membrane function. J Am Soc Nephrol 2001, 12:2029-39.

[9] Selgas R, Bajo A, Jiménez-Heffernan JA, Sánchez-Tomero JA, Del Peso G, Aguilera A, López-Cabrera M: Epithelial-to-mesenchymal transition of the mesothelial cell--its role in the response of the peritoneum to dialysis. Nephrol Dial Transplant 2006, 21 Suppl 2:ii2-7.

[10] Landgraf P, Rusu M, Sheridan R, Sewer A, Iovino N, Aravin A, Pfeffer S, Rice A, Kamphorst AO, Landthaler M, Lin C, Socci ND, Hermida L, Fulci V, Chiaretti S, Foà R, Schliwka J, Fuchs U, Novosel A, Müller RU, Schermer B, Bissels U, Inman J, Phan Q, Chien M, Weir DB, Choksi R, De Vita G, Frezzetti D, Trompeter HI, Hornung V, Teng G, Hartmann G, Palkovits M, Di Lauro R, Wernet P, Macino G, Rogler CE, Nagle JW, Ju J, Papavasiliou FN, Benzing T, Lichter P, Tam W, Brownstein MJ, Bosio A, Borkhardt A, Russo JJ, Sander C, Zavolan M, Tuschl T: A mammalian microRNA expression atlas based on small RNA library sequencing. Cell 2007, 129:1401-14.

[11] Brown BD, Naldini L: Exploiting and antagonizing microRNA regulation for therapeutic and experimental applications. Nat Rev Genet 2009, 10:578-85.

[12] Cortez MA, Bueso-Ramos C, Ferdin J, Lopez-Berestein G, Sood AK, Calin GA: MicroRNAs in body fluids--the mix of hormones and biomarkers. Nat Rev Clin Oncol 2011, 8:467-77.

[13] Kota J, Chivukula RR, O'Donnell KA, Wentzel EA, Montgomery CL, Hwang HW, Chang TC, Vivekanandan P, Torbenson M, Clark KR, Mendell JR, Mendell JT: Therapeutic microRNA delivery suppresses tumorigenesis in a murine liver cancer model. Cell 2009, 137:1005-17.

[14] Turchinovich A, Weiz L, Langheinz A, Burwinkel B: Characterization of extracellular circulating microRNA. Nucleic Acids Res 2011, 39:7223-33.

[15] Lopez-Anton M, Bowen T, Jenkins HR: microRNA Regulation of Peritoneal Cavity Homeostasis in Peritoneal Dialysis. BioMed Research International 2015.

[16] Chen J, Kam-Tao P, Kwan BC, Chow KM, Lai KB, Luk CC, Szeto CC: Relation between microRNA expression in peritoneal dialysis effluent and peritoneal transport characteristics. Dis Markers 2012, 33:35-42.
[17] Zhou Q, Yang M, Lan H, Yu X: miR-30a negatively regulates TGF-β1-induced epithelial-mesenchymal transition and peritoneal fibrosis by targeting Snai1. Am J Pathol 2013, 183:808-19.
[18] Ohkubo T, Ozawa M: The transcription factor Snail downregulates the tight junction components independently of E-cadherin downregulation. J Cell Sci 2004, 117:1675-85.
[19] Kurrey NK, K A, Bapat SA: Snail and Slug are major determinants of ovarian cancer invasiveness at the transcription level. Gynecol Oncol 2005, 97:155-65.
[20] Zhang K, Zhang H, Zhou X, Tang WB, Xiao L, Liu YH, Liu H, Peng YM, Sun L, Liu FY: miRNA589 regulates epithelial-mesenchymal transition in human peritoneal mesothelial cells. J Biomed Biotechnol 2012, 2012:673096.
[21] Zhang L, Liu F, Peng Y, Sun L, Chen G: Changes in expression of four molecular marker proteins and one microRNA in mesothelial cells of the peritoneal dialysate effluent fluid of peritoneal dialysis patients. Exp Ther Med 2013, 6:1189-93.
[22] Stylianou E, Jenner LA, Davies M, Coles GA, Williams JD: Isolation, culture and characterization of human peritoneal mesothelial cells. Kidney Int 1990, 37:1563-70.
[23] Yung S, Li FK, Chan TM: Peritoneal mesothelial cell culture and biology. Perit Dial Int 2006, 26:162-73.
[24] Lambie M, Chess J, Donovan KL, Kim YL, Do JY, Lee HB, Noh H, Williams PF, Williams AJ, Davison S, Dorval M, Summers A, Williams JD, Bankart J, Davies SJ, Topley N, Investigators GFS: Independent effects of systemic and peritoneal inflammation on peritoneal dialysis survival. J Am Soc Nephrol 2013, 24:2071-80.
[25] Peltier HJ, Latham GJ: Normalization of microRNA expression levels in quantitative RT-PCR assays: identification of suitable reference RNA targets in normal and cancerous human solid tissues. RNA 2008, 14:844-52.
[26] Livak KJ, Schmittgen TD: Analysis of relative gene expression data using real-time quantitative PCR and the 2(-Delta Delta C(T)) Method. Methods 2001, 25:402-8.
[27] Jang YH, Shin HS, Sun Choi H, Ryu ES, Jin Kim M, Ki Min S, Lee JH, Kook Lee H, Kim KH, Kang DH: Effects of dexamethasone on the TGF-β1-induced epithelial-to-mesenchymal transition in human peritoneal mesothelial cells. Lab Invest 2013, 93:194-206.
[28] Xiao L, Peng X, Liu F, Tang C, Hu C, Xu X, Wang M, Luo Y, Yang S, Song P, Xiao P, Kanwar YS, Sun L: AKT regulation of mesothelial-to-mesenchymal transition in peritoneal dialysis is modulated by Smurf2 and deubiquitinating enzyme USP4. BMC Cell Biol 2015, 16:7.
[29] Xiao L, Zhou X, Liu F, Hu C, Zhu X, Luo Y, Wang M, Xu X, Yang S, Kanwar YS, Sun L: MicroRNA-129-5p modulates epithelial-to-mesenchymal transition by targeting SIP1 and SOX4 during peritoneal dialysis. Lab Invest 2015.
[30] Ruiz-Carpio V, Sandoval P, Aguilera A, Albar-Vizcaíno P, Perez-Lozano ML, González-Mateo GT, Acuña-Ruiz A, García-Cantalejo J, Botías P, Bajo MA, Selgas R, Sánchez-Tomero JA, Passlick-Deetjen J, Piecha D, Büchel J, Steppan S, López-Cabrera M: Genomic reprograming analysis of the Mesothelial to Mesenchymal Transition identifies bioma rkers in peritoneal dialysis patients. Scientific Reports (In press) 2017.
[31] Jenkins RH, Davies LC, Taylor PR, Akiyama H, Cumbes B, Beltrami C, Carrington CP, Phillips AO, Bowen T, Fraser DJ: miR-192 induces G2/M growth arrest in aristolochic acid nephropathy. Am J Pathol 2014, 184:996-1009.
[32] Heller F, Lindenmeyer MT, Cohen CD, Brandt U, Draganovici D, Fischereder M, Kretzler M, Anders HJ, Sitter T, Mosberger I, Kerjaschki D, Regele H, Schlöndorff D, Segerer S: The contribution of B cells to renal interstitial inflammation. Am J Pathol 2007, 170:457-68.
[33] Medina I, Carbonell J, Pulido L, Madeira SC, Goetz S, Conesa A, Tárraga J, Pascual-Montano A, Nogales-Cadenas R, Santoyo J, García F, Marbà M, Montaner D, Dopazo J: Babelomics: an

integrative platform for the analysis of transcriptomics, proteomics and genomic data with advanced functional profiling. Nucleic Acids Res 2010, 38:W210-3.
[34] Asangani IA, Rasheed SAK, Nikolova DA, Leupold JH, Colburn NH, Post S, Allgayer H: MicroRNA-21 (miR-21) post-transcriptionally downregulates tumor suppressor Pdcd4 and stimulates invasion, intravasation and metastasis in colorectal cancer. Oncogene 2008, 27:2128-36.
[35] Yao Q, Cao S, Li C, Mengesha A, Kong B, Wei M: Micro-RNA-21 regulates TGF-β-induced myofibroblast differentiation by targeting PDCD4 in tumor-stroma interaction. Int J Cancer 2011, 128:1783-92.
[36] Brønnum H, Andersen DC, Schneider M, Sandberg MB, Eskildsen T, Nielsen SB, Kalluri R, Sheikh SP: miR-21 promotes fibrogenic epithelial-to-mesenchymal transition of epicardial mesothelial cells involving Programmed Cell Death 4 and Sprouty-1. PLoS One 2013, 8:e56280.
[37] Fielding CA, Jones GW, McLoughlin RM, McLeod L, Hammond VJ, Uceda J, Williams AS, Lambie M, Foster TL, Liao CT, Rice CM, Greenhill CJ, Colmont CS, Hams E, Coles B, Kift-Morgan A, Newton Z, Craig KJ, Williams JD, Williams GT, Davies SJ, Humphreys IR, O'Donnell VB, Taylor PR, Jenkins BJ, Topley N, Jones SA: Interleukin-6 signaling drives fibrosis in unresolved inflammation. Immunity 2014, 40:40-50.
[38] Paraskevopoulou MD, Georgakilas G, Kostoulas N, Vlachos IS, Vergoulis T, Reczko M, Filippidis C, Dalamagas T, Hatzigeorgiou AG: DIANA-microT web server v5.0: service integration into miRNA functional analysis workflows. Nucleic Acids Res 2013, 41:W169-73.
[39] Reczko M, Maragkakis M, Alexiou P, Grosse I, Hatzigeorgiou AG: Functional microRNA targets in protein coding sequences. Bioinformatics 2012, 28:771-6.
[40] Wong N, Wang X: miRDB: an online resource for microRNA target prediction and functional annotations. Nucleic Acids Res 2015, 43:D146-52.
[41] Wang X, El Naqa IM: Prediction of both conserved and nonconserved microRNA targets in animals. Bioinformatics 2008, 24:325-32.
[42] Betel D, Koppal A, Agius P, Sander C, Leslie C: Comprehensive modeling of microRNA targets predicts functional non-conserved and non-canonical sites. Genome Biol 2010, 11:R90.
[43] Betel D, Wilson M, Gabow A, Marks DS, Sander C: The microRNA.org resource: targets and expression. Nucleic Acids Res 2008, 36:D149-53.
[44] Agarwal V, Bell GW, Nam JW, Bartel DP: Predicting effective microRNA target sites in mammalian mRNAs. Elife 2015, 4.
[45] Nam JW, Rissland OS, Koppstein D, Abreu-Goodger C, Jan CH, Agarwal V, Yildirim MA, Rodriguez A, Bartel DP: Global analyses of the effect of different cellular contexts on microRNA targeting. Mol Cell 2014, 53:1031-43.
[46] Bartel DP: MicroRNAs: target recognition and regulatory functions. Cell 2009, 136:215-33.
[47] Beltrami C, Clayton A, Phillips AO, Fraser DJ, Bowen T: Analysis of urinary microRNAs in chronic kidney disease. Biochem Soc Trans 2012, 40:875-9.
[48] Williams JD, Craig KJ, Topley N, Von Ruhland C, Fallon M, Newman GR, Mackenzie RK, Williams GT, Group PBS: Morphologic changes in the peritoneal membrane of patients with renal disease. J Am Soc Nephrol 2002, 13:470-9.
[49] Lopes Barreto D, Krediet RT: Current status and practical use of effluent biomarkers in peritoneal dialysis patients. Am J Kidney Dis 2013, 62:823-33.
[50] Moriishi M, Kawanishi H: Icodextrin and intraperitoneal inflammation. Perit Dial Int 2008, 28 Suppl 3:S96-S100.
[51] Velloso MS, Otoni A, de Paula Sabino A, de Castro WV, Pinto SW, Marinho MA, Rios DR: Peritoneal dialysis and inflammation. Clin Chim Acta 2014, 430:109-14.
[52] McLoughlin RM, Witowski J, Robson RL, Wilkinson TS, Hurst SM, Williams AS, Williams JD, Rose-John S, Jones SA, Topley N: Interplay between IFN-gamma and IL-6 signaling governs neutrophil trafficking and apoptosis during acute inflammation. J Clin Invest 2003, 112:598-607.

[53] Topley N, Jörres A, Luttmann W, Petersen MM, Lang MJ, Thierauch KH, Müller C, Coles GA, Davies M, Williams JD: Human peritoneal mesothelial cells synthesize interleukin-6: induction by IL-1 beta and TNF alpha. Kidney Int 1993, 43:226-33.
[54] Witowski J, Jörres A, Coles GA, Williams JD, Topley N: Superinduction of IL-6 synthesis in human peritoneal mesothelial cells is related to the induction and stabilization of IL-6 mRNA. Kidney Int 1996, 50:1212-23.
[55] Löffler D, Brocke-Heidrich K, Pfeifer G, Stocsits C, Hackermüller J, Kretzschmar AK, Burger R, Gramatzki M, Blumert C, Bauer K, Cvijic H, Ullmann AK, Stadler PF, Horn F: Interleukin-6 dependent survival of multiple myeloma cells involves the Stat3-mediated induction of microRNA-21 through a highly conserved enhancer. Blood 2007, 110:1330-3.
[56] Lu X, Luo F, Liu Y, Zhang A, Li J, Wang B, Xu W, Shi L, Liu X, Lu L, Liu Q: The IL-6/STAT3 pathway via miR-21 is involved in the neoplastic and metastatic properties of arsenite-transformed human keratinocytes. Toxicol Lett 2015, 237:191-9.
[57] Iliopoulos D, Jaeger SA, Hirsch HA, Bulyk ML, Struhl K: STAT3 activation of miR-21 and miR-181b-1 via PTEN and CYLD are part of the epigenetic switch linking inflammation to cancer. Mol Cell 2010, 39:493-506.
[58] Chen M, Liu Y, Varley P, Chang Y, He XX, Huang H, Tang D, Lotze MT, Lin J, Tsung A: High-Mobility Group Box 1 Promotes Hepatocellular Carcinoma Progression through miR-21-Mediated Matrix Metalloproteinase Activity. Cancer Res 2015, 75:1645-56.
[59] Zhou X, Ren Y, Liu A, Han L, Zhang K, Li S, Li P, Kang C, Wang X, Zhang L: STAT3 inhibitor WP1066 attenuates miRNA-21 to suppress human oral squamous cell carcinoma growth in vitro and in vivo. Oncol Rep 2014, 31:2173-80.
[60] Usui H, Shibayama M, Ohbayashi N, Konishi M, Takada S, Itoh N: Fgf18 is required for embryonic lung alveolar development. Biochem Biophys Res Commun 2004, 322:887-92.
[61] Franco-Montoya ML, Boucherat O, Thibault C, Chailley-Heu B, Incitti R, Delacourt C, Bourbon JR: Profiling target genes of FGF18 in the postnatal mouse lung: possible relevance for alveolar development. Physiol Genomics 2011, 43:1226-40.
[62] Surette AP, Madureira PA, Phipps KD, Miller VA, Svenningsson P, Waisman DM: Regulation of fibrinolysis by S100A10 in vivo. Blood 2011, 118:3172-81.
[63] Piecha D, Wiberg C, Mörgelin M, Reinhardt DP, Deák F, Maurer P, Paulsson M: Matrilin-2 interacts with itself and with other extracellular matrix proteins. Biochem J 2002, 367:715-21.
[64] Ichikawa T, Suenaga Y, Koda T, Ozaki T, Nakagawara A: DeltaNp63/BMP-7-dependent expression of matrilin-2 is involved in keratinocyte migration in response to wounding. Biochem Biophys Res Commun 2008, 369:994-1000.
[65] Tam CW, Liu VW, Leung WY, Yao KM, Shiu SY: The autocrine human secreted PDZ domain-containing protein 2 (sPDZD2) induces senescence or quiescence of prostate, breast and liver cancer cells via transcriptional activation of p53. Cancer Lett 2008, 271:64-80.
[66] Termén S, Tan EJ, Heldin CH, Moustakas A: p53 regulates epithelial-mesenchymal transition induced by transforming growth factor β. J Cell Physiol 2013, 228:801-13.
[67] Yeung ML, Tam TS, Tsang AC, Yao KM: Proteolytic cleavage of PDZD2 generates a secreted peptide containing two PDZ domains. EMBO Rep 2003, 4:412-8.

Figure Legends

Figure 1. miRNA profiling in TGF-β1-stimulated HPMCs and miRNA changes confirmation in *in vitro* and *ex vivo* models. **(A)** Three-dimensional scatter plot of miRNA expression following 1ng/ml of TGF-β1-treatment for 48 h (x axis: $\log_2$ fold change of the normalized miRNA signal (mean of at least three replicates); y axis: $-\log_{10}$ p value obtained from one-way analysis of the variance (ANOVA) followed by Fisher's least significant difference (LSD) post hoc analysis; z axis: $\log_{10}$ of the level of baseline expression in mesothelial cells). **(B)** miR-21 expression validation. Control - white bars, TGF-β1 (1ng/ml, 48 h) – black bars. **(C)** Relative expression of miR-21 in control omentum-derived mesothelial cells (HPMCs), TGF-β1 treated (1ng/ml, 48h) and cultured peritoneal effluent derived (PDE) cells with epithelial (E) and non-epithelial (NE) phenotype. Expression of miR-21 was analyzed by RT-qPCR and normalized to miR-191 expression. Data were analyzed by paired *t* test or one- way ANOVA followed by post-hoc Holm-Sidak's test comparing each condition mean with the control omentum-derived mean. Data represent the mean S.E.M. from five independent donor experiments. *$p < 0.05$.

Figure 2. miR-21 expression is up-regulated at the peritoneal membrane in peritoneal dialysis patients. Formalin-fixed paraffin embedded (FFPE) samples were stained for p-SMAD2/3 **(A-C)** and PDCD4 **(E-G)**, and manually macro-dissected to measure relative expression of miR-21 **(D)** from a total of 44 patients. **(A)** Histological image analysis using Aperio Precision Image Analysis Software. Mesothelial and submesothelial compact zone selection (upper panel) and p-SMAD2/3 detection of the area of interest by the Aperio positive pixel count algorithm (lower panel). Negative background (blue), positive p-SMAD2/3 detection (yellow-orange). Scale bar, 300 μm. **(B)** Higher

magnification image to demonstrate nuclear immunostaining of p-SMAD2/3 and negative control. Scale bar, 50 µm. **(C)** P-SMAD2/3 up-regulation. Level of p-SMAD2/3 staining was defined using a count algorithm for positive pixel detection. **(D)** miR-21 expression. miR-21 expression was analysed by RT-qPCR and normalized to miR-191 expression. **(E-G)** Formalin-fixed paraffin embedded (FFPE) samples were PDCD4 stained. **(E)** Histological image analysis using Aperio Precision Image Analysis Software. Mesothelial and submesothelial compact zone was selected as area of interest and PDCD4 staining was quantified by the aperio positive pixel count algorithm. **(F)** PDCD4 negative control. **(G)** Positive PDCD4 detection (brown). Scale bar, 80 µm. Data were analyzed by one-way ANOVA followed by post-hoc Holm-Sidak's test comparing all condition means. Data represent the mean S.E.M. from eleven age-matched samples and equal average PD duration between PD groups (n=44). *$p < 0.05$; ***$p < 0.005$; ****$p < 0.001$; *****$p < 0.0005$.

Figure 3. miR-21 expression in peritoneal dialysis effluent (PDE) from PD patients (n=230). RNA from 230 PDE samples was isolated and relative expression of miR-21 was normalized to miR-191 expression. **(A)** Up-regulation of miR-21 expression in peritoneal dialysis effluent (PDE) from prevalent PD patients compared with incident cases. Data were analyzed by unpaired, Mann-Whitney test. Data represent the mean S.E.M. from samples. ***$p < 0.005$. **(B)** Effect of IL-6 and IFN-γ on miR-21 prediction levels. The predicted variable, miR-21, was log transformed. (n=230).

Figure 4. Mesothelial to mesenchymal mRNA array changes associated to PD therapy in HPMCs and *In silico* target prediction to identify new miR-21 targets that may contribute to the process. **(A)** Diagram displaying mRNA array changes comparing control omentum HPMCs and PDE derived MCs with epithelial phenotype (early-MMT,

green), PDE derived MCs with epithelial phenotype and non-epithelial phenotype (late-MMT, yellow), and control omentum HPMCs and PDE derived MCs with non-epithelial phenotype (whole-MMT, red). **(B)** miR-21 target prediction using Diana (blue), miRDB (brown), miRanda (green) and TargetScan (red) inter-crossed using Venn diagram to identify targets that were predicted by three or more algorithms. **(C)** Diagram displaying miR-21 targets predicted and identified in **(B)** further inter-crossed using Venn diagram with the mRNA array changes identified in (**A**; green, yellow, red). Common targets identified by **(A)** and **(B)** inter-crossed lists are shown into squares with the respective MMT color (top left, early-MMT; top right, late-MMT; bottom, whole-MMT).

Figure 5. Predicted miR-21 target profiling in a model of progressive peritoneal membrane deterioration. **(A-N)** Relative mRNA expression in control omentum-derived mesothelial cells (HPMCs), TGF-β1 treated (1ng/ml, 48h) and cultured peritoneal effluent derived (PDE) cells with epithelial (E) and non-epithelial (NE) phenotype (n=5 for each group). **(A)** *NPPB*. **(B)** *PDZD2*. **(C)** *S100A10*. **(D)** *SASH1*. **(E)** *TIMP3*. **(F)** *AIM1L*. **(G)** *CASKIN1*. **(H)** *DUSP8*. **(I)** *FGF18*. **(J)** *MATN2*. **(K)** *NELL2*. **(L)** *RHOB*. **(M)** *SPRY1*. **(N)** *PDCD4* **(A-N)** Target gene expression was analyzed by RT-qPCR and normalized to GAPDH. Data were analyzed by no matched one-way ANOVA followed by post-hoc Holm-Sidak's test. Data represent the mean S.E.M. from five independent donor experiments. *$p < 0.05$; **$p < 0.01$; ***$p < 0.005$; ****$p < 0.001$.

Figure 6. miR-21 target mRNA expression 48h after miRNA mimic **(A, C, E, G, I)** or inhibitor **(B, D, F, H, J)** delivery in HPMCs at concentrations 5-20pM as indicated. miR-control (mimic or inhibitor) – white bars, miR-21 mimic – black bars, miR-21 inhibitor – grey bars. **(A, B)** *PDZD2*. **(C, D)** *S100A10*. **(E, F)** *FGF18*. **(G, H)** *MATN2.* **(I, J)** *PDCD4.*

Target gene expression was analyzed by RT-qPCR and normalized to *GAPDH* expression. Data were analyzed by matched factor two-way ANOVA followed by post-hoc Holm-Sidak's test. Data represent the mean S.E.M. from three (miRNA mimic) and six (miRNA inhibitor) independent donor experiments. *$p < 0.05$; **$p < 0.01$; ***$p < 0.005$; ****$p < 0.001$.

Main Tables

Symbol	Reverse and Forward Primers (5'-3')
E-Cadherin	F: 5□ TCCCAATACATCTCCCTTCACA 3□ R: 5□ ACCCACCTCTAAGGCCATCTTT 3□
ZO-1	F: 5□ GGAGAGGTGTTCCGTGTTGT 3□ R: 5□ GGCTAGCTGCTCAGCTCTGT 3□
Occludin	F: 5□ TAAATCCACGCCGGTTCCTGAAGT 3□ R: 5□ AGGTGTCTCAAAGTTACCACCGCT 3□
Claudin-1	F: 5□ CGGGTTGCTTGCAATGTGC 3□ R: 5□ CCGGCGACAACATCGTGAC 3□
Fibronectin	F: 5□ CCGAGGTTTTAACTGCGAGA 3□ R: 5□ TCACCCACTCGGTAAGTGTTC 3□
Collagen1a1	F: 5□ CATGTTCAGCTTTGTGGACCTC 3□ R: 5□ TTGGTGGGATGTCTTCGTCT 3□
Snail	F: 5□ TTTACCTTCCAGCAGCCCTA 3□ R: 5□ GGACAGAGTCCCAGATGAGC 3□
α-SMA	F: 5□ AACTGGGACGACATGGAAA 3□ R: 5□ AGGGTGGGATGCTCTTCAG 3□
GAPDH	F: 5□ CCTCTGACTTCAACAGCGACAC 3□ R: 5□ TGTCATACCAGGAAATGAGCTTGA 3□
PDCD4	F: 5□ TGGATTAACTGTGCCAACCA 3□ R: 5□ TCTCAAATGCCCTTTCATCC 3□
SPRY1	F: 5□ AGATGCATGCCAGGTTTCCA 3□ R: 5□ TAACGAACTGCCACTGCCAT 3□
PTEN	F: 5□ CGGCAGCATCAAATGTTTCAG 3□ R: 5□ AACTGGCAGGTAGAAGGCAACTC 3□
LATS2	F: 5□ CAGATTCAGACCTCTCCCGT 3□ R: 5□ CTTAAAGGCGTATGGCGAGT 3□

STK40	F: 5□ CCAGTGCCCTTGCCTCATAA 3□ R: 5□ AATCTCGGCTCAAAAGGGCA 3□

Table 1: RT-qPCR Primer Sequences. Primer sequences designed and used for RT-qPCR in this study.

Variable	Coefficient (95% Confidence Interval)	p value
Icodextrin Usage	0.52 (0.20, 0.84)	0.002
Peritonitis Count	0.16 (0.03, 0.29)	0.015
Dialysate IL-6	0.28 (-0.02, 0.58)	0.065
Dialysate TNF-α	0.86 (-0.61, 2.34)	0.25
Dialysate IFN-γ	-0.77 (-1.21, -0.33)	0.001
Dialysate IL-1β	0.69 (-0.89, 2.27)	0.39
Body Mass Index	0.027 (-0.0004, 0.054)	0.053

Table 2: Multivariable Regression of miR-21. Multivariable linear regression with backwards stepwise variable selection for parameters listed in Supplemental Table 2.

FIGURE 1

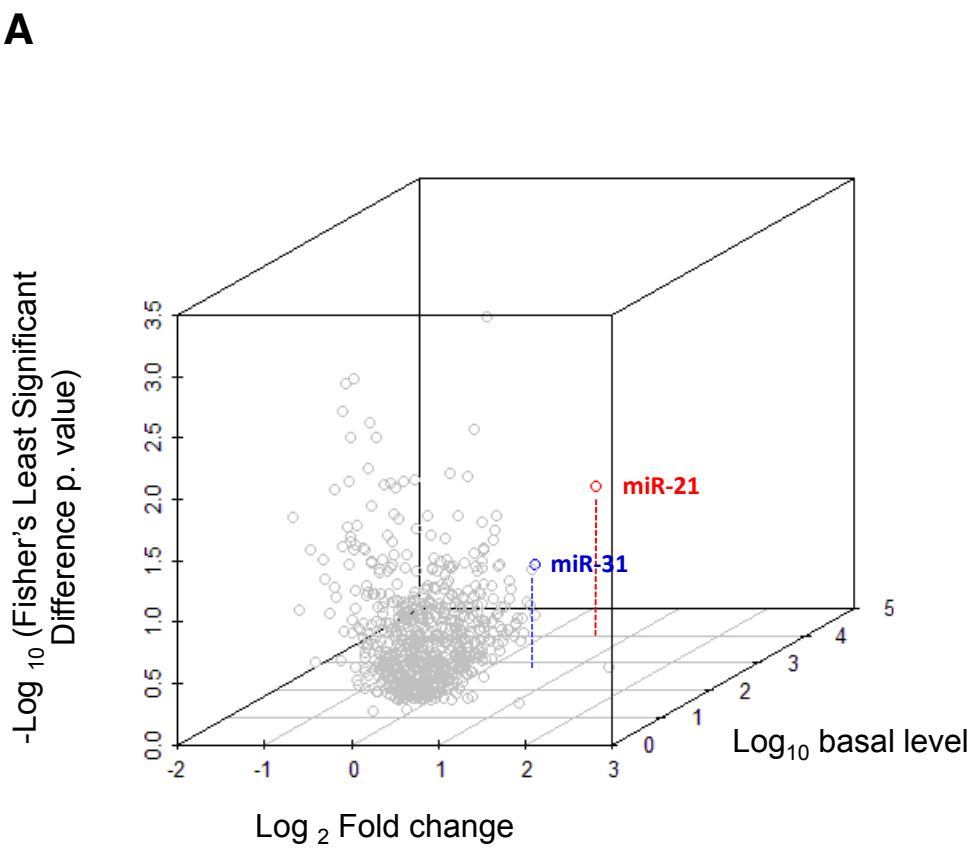
A
-Log 10 (Fisher's Least Significant Difference p. value)
miR-21
miR-31
Log 2 Fold change
Log10 basal level

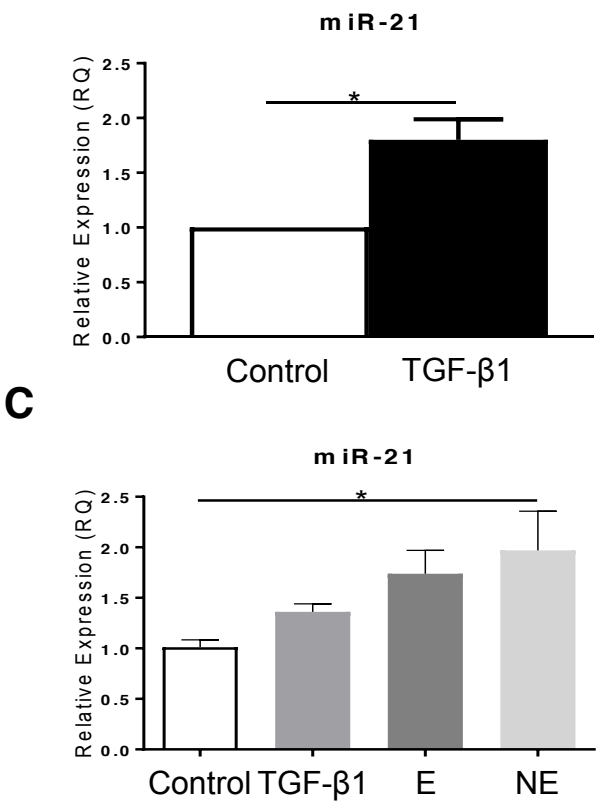
B
miR-21
Relative Expression (RQ)
Control
TGF-β1
C
miR-21
Relative Expression (RQ)
Control
TGF-β1
E
NE

FIGURE 2

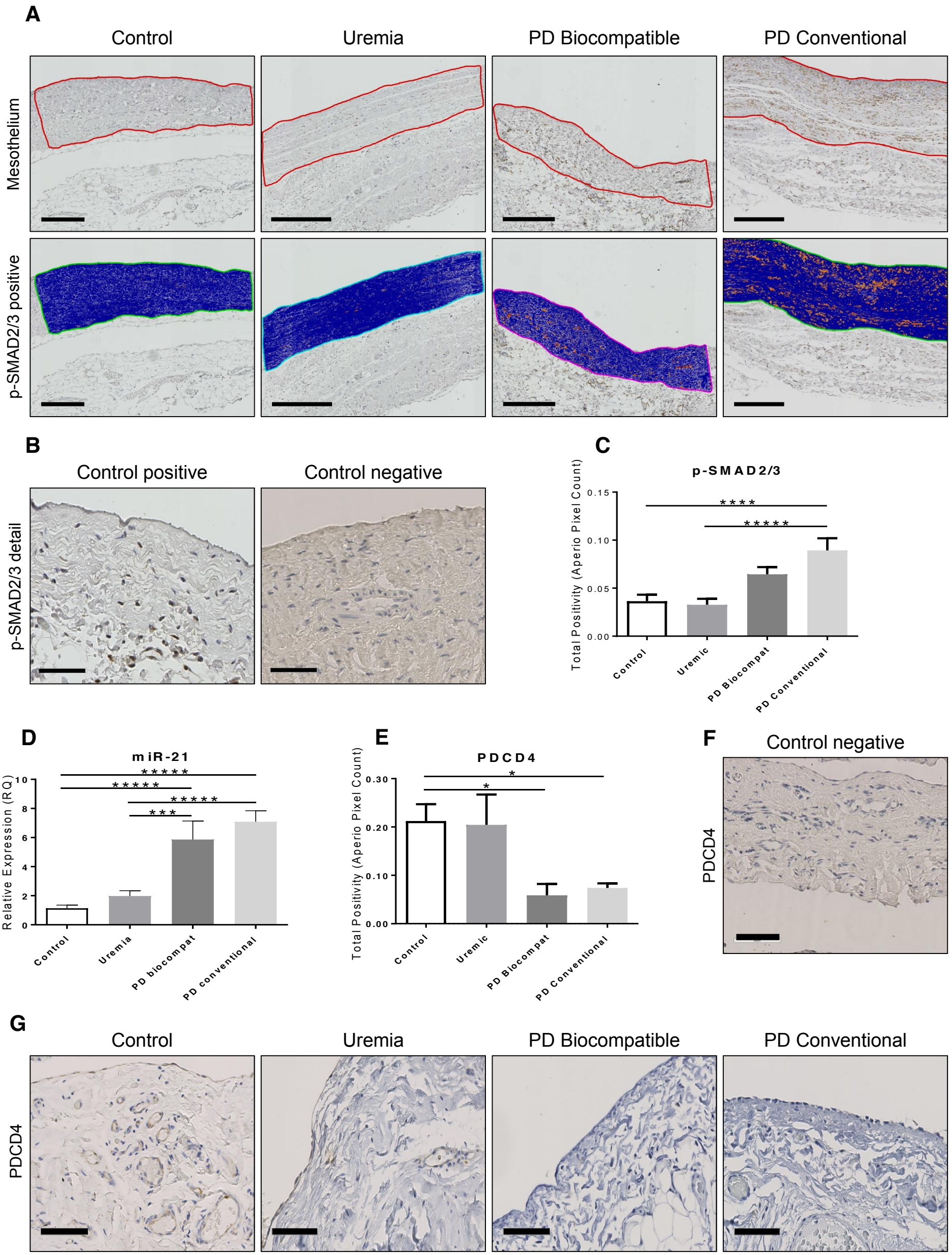
A
Control
Uremia
PD Biocompatible
PD Conventional
Mesothelium
p-SMAD2/3 positive
B
Control positive
Control negative
p-SMAD2/3 detail
C
p-SMAD2/3
Total Positivity (Aperio Pixel Count)
0.15
0.10
0.05
0.00
****
*****
Control
Uremic
PD Biocompat
PD Conventional
D
miR-21
Relative Expression (RQ)
10
8
6
4
2
0
*****
*****
*****
***
Control
Uremia
PD biocompat
PD conventional
E
PDCD4
Total Positivity (Aperio Pixel Count)
0.30
0.20
0.10
0.00
*
*
Control
Uremic
PD Biocompat
PD Conventional
F
Control negative
PDCD4
G
Control
Uremia
PD Biocompatible
PD Conventional
PDCD4

FIGURE 3

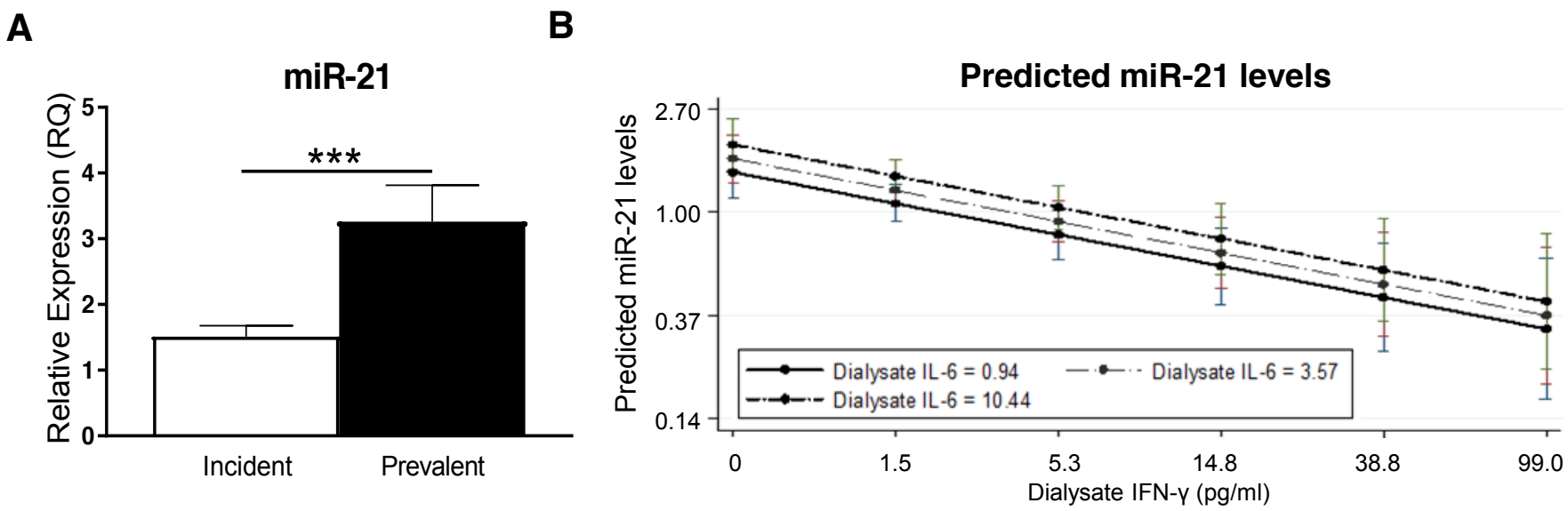
A
miR-21
Relative Expression (RQ)
5
4
3
2
1
0
***
Incident
Prevalent
B
Predicted miR-21 levels
Predicted miR-21 levels
2.70
1.00
0.37
0.14
Dialysate IL-6 = 0.94
Dialysate IL-6 = 3.57
Dialysate IL-6 = 10.44
0
1.5
5.3
14.8
38.8
99.0
Dialysate IFN-γ (pg/ml)

FIGURE 4

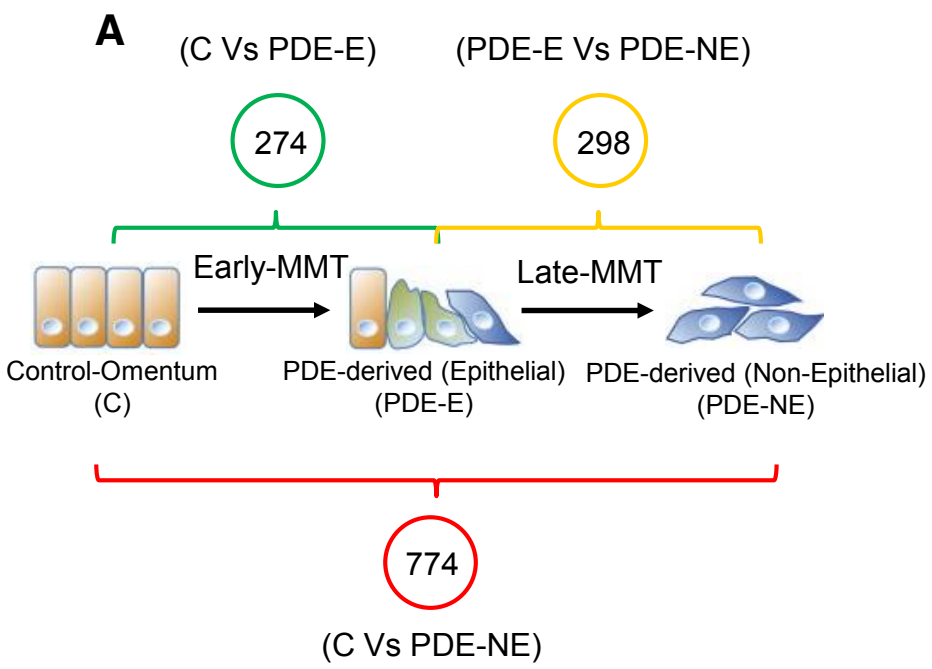
A
(C Vs PDE-E)
(PDE-E Vs PDE-NE)
274
298
Early-MMT
Late-MMT
Control-Omentum
(C)
PDE-derived (Epithelial)
(PDE-E)
PDE-derived (Non-Epithelial)
(PDE-NE)
774
(C Vs PDE-NE)

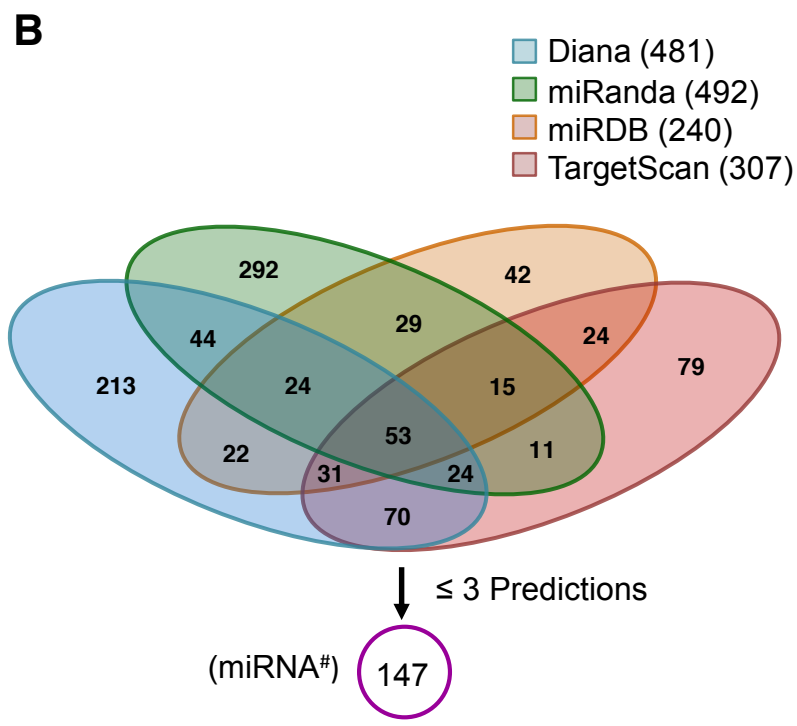
B
Diana (481)
miRanda (492)
miRDB (240)
TargetScan (307)
292
42
44
29
24
213
24
15
79
53
22
11
31
24
70
≤ 3 Predictions
(miRNA#)
147

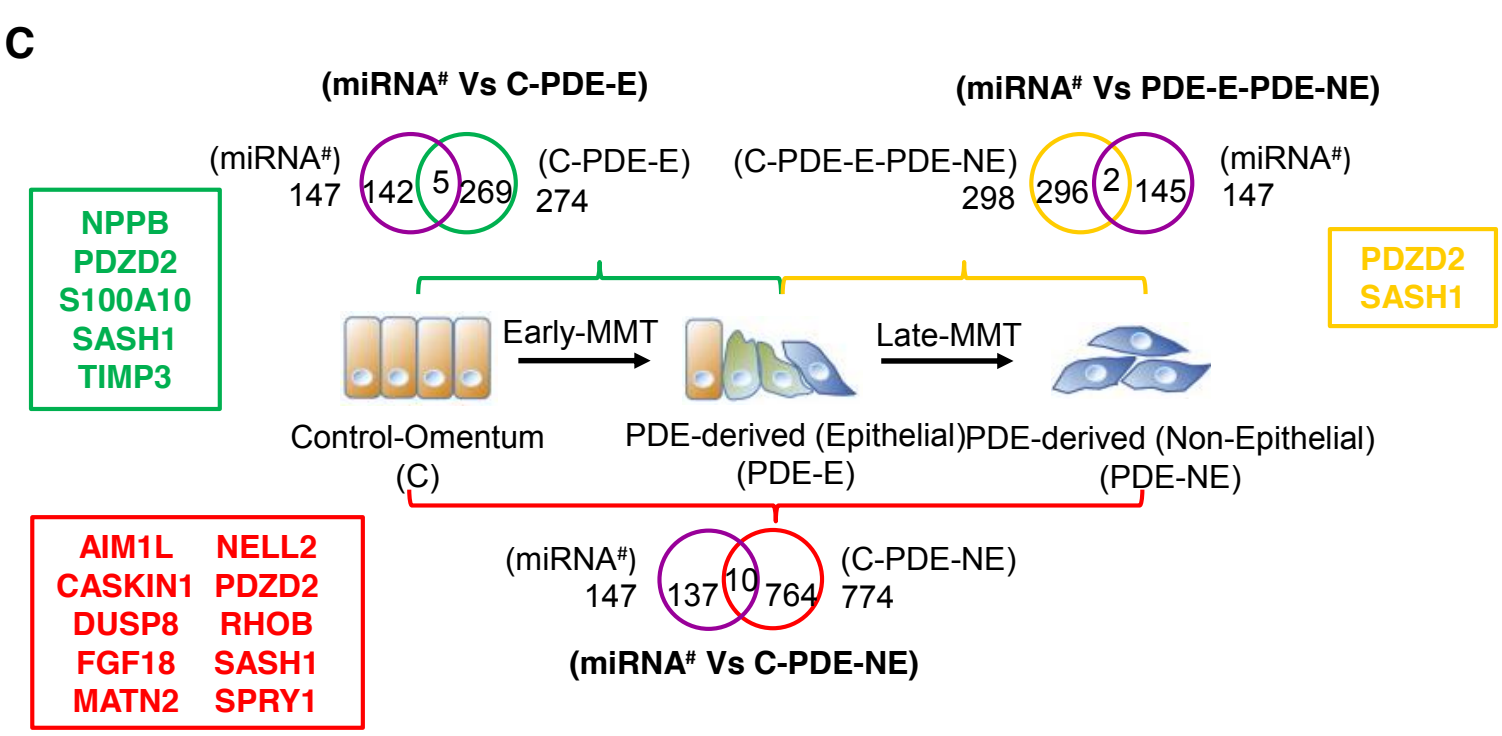
C
(miRNA# Vs C-PDE-E)
(miRNA#)
147
142
5
269
(C-PDE-E)
274
(C-PDE-E-PDE-NE)
298
296
2
145
(miRNA#)
147
(miRNA# Vs PDE-E-PDE-NE)
NPPB
PDZD2
S100A10
SASH1
TIMP3
PDZD2
SASH1
Early-MMT
Late-MMT
Control-Omentum
(C)
PDE-derived (Epithelial)
(PDE-E)
PDE-derived (Non-Epithelial)
(PDE-NE)
AIM1L
CASKIN1
DUSP8
FGF18
MATN2
NELL2
PDZD2
RHOB
SASH1
SPRY1
(miRNA#)
147
137
10
764
(C-PDE-NE)
774
(miRNA# Vs C-PDE-NE)

FIGURE 5

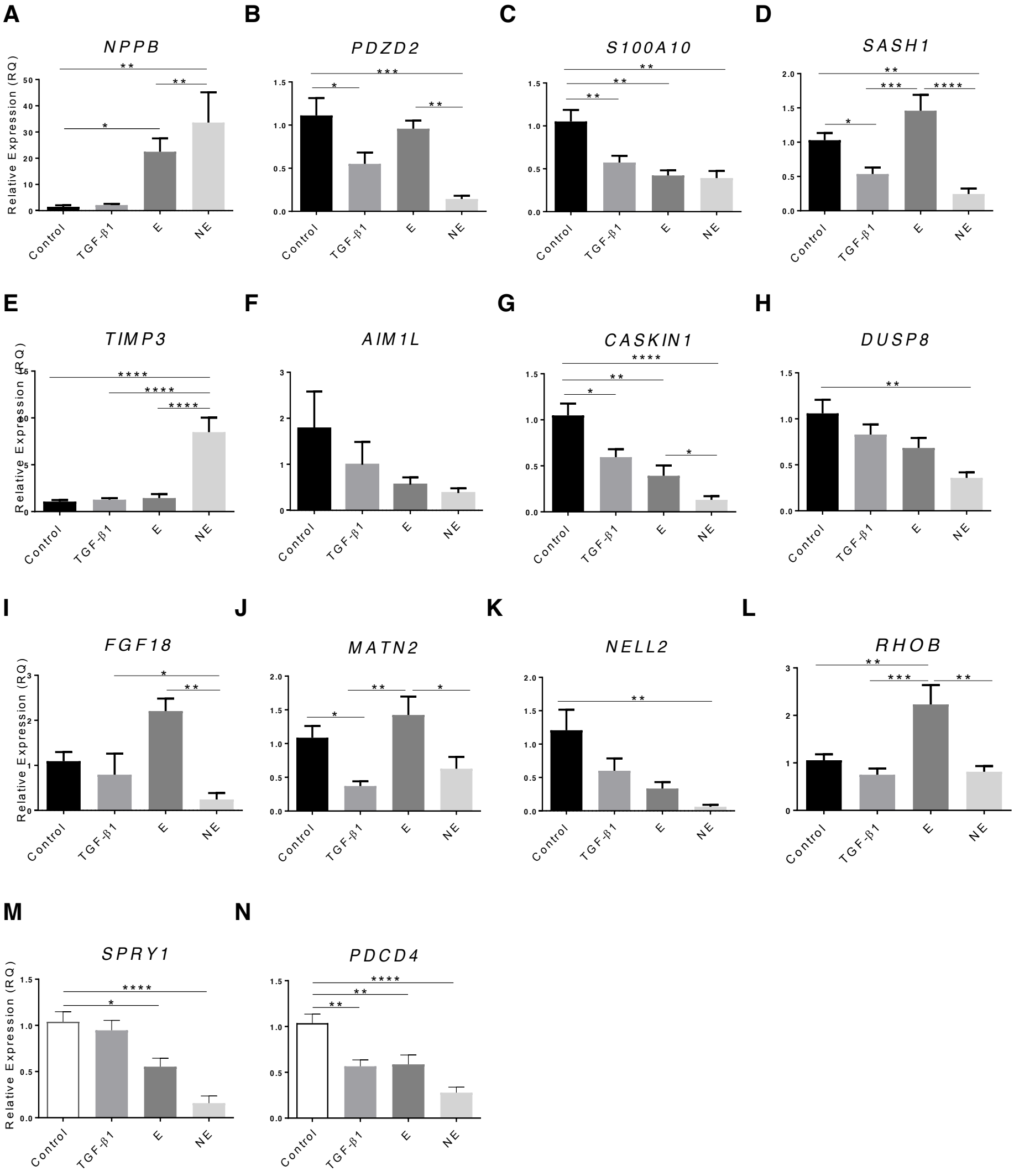
A
NPPB
B
PDZD2
C
S100A10
D
SASH1
E
TIMP3
F
AIM1L
G
CASKIN1
H
DUSP8
I
FGF18
J
MATN2
K
NELL2
L
RHOB
M
SPRY1
N
PDCD4
Relative Expression (RQ)
Control
TGF-β1
E
NE

FIGURE 6

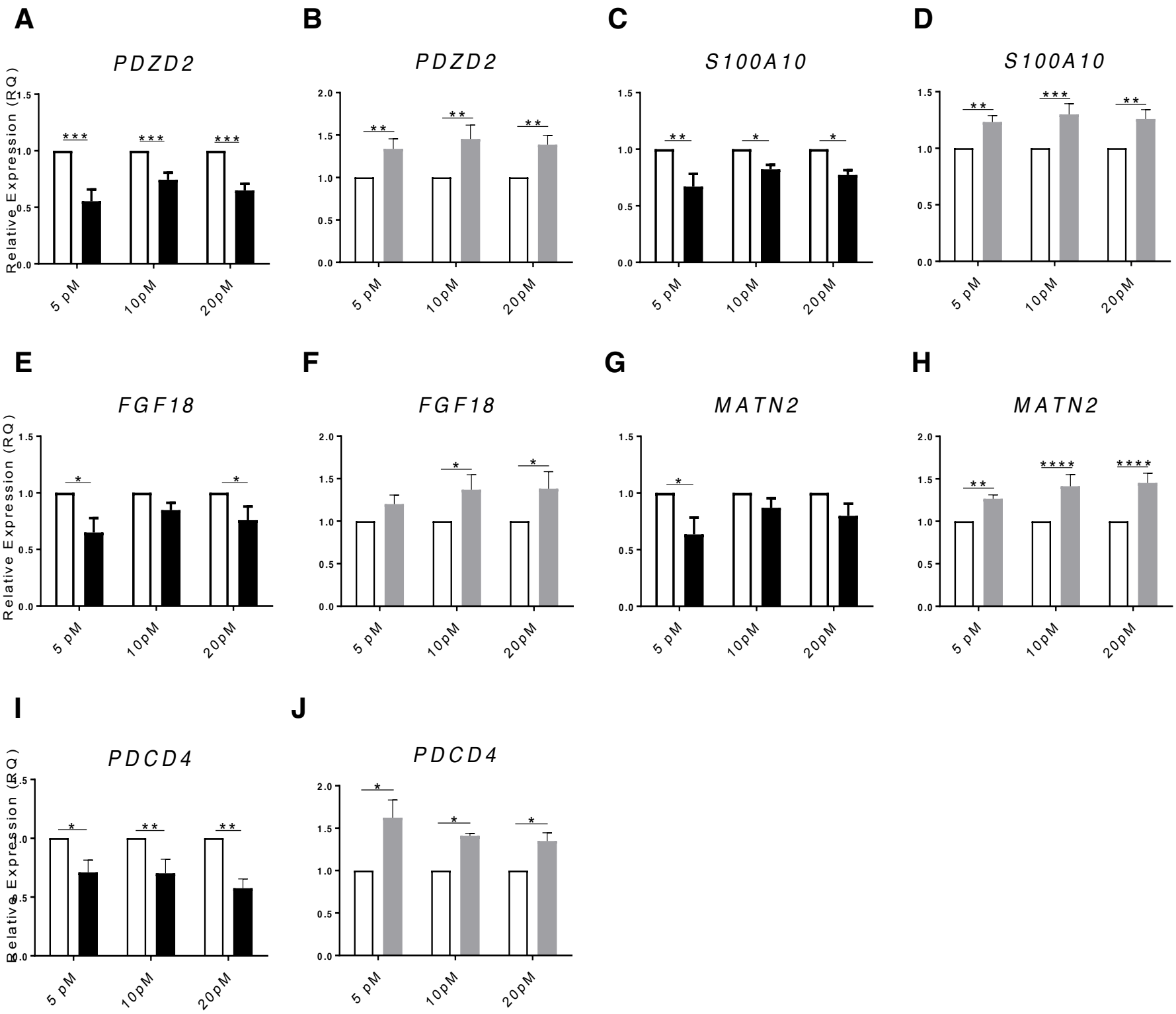
A
PDZD2
B
PDZD2
C
S100A10
D
S100A10
E
FGF18
F
FGF18
G
MATN2
H
MATN2
I
PDCD4
J
PDCD4
Relative Expression (RQ)
5 pM
10pM
20pM

Supplemental Figure Legends

Supplemental Figure 1. TGF-β1 represses epithelial and induces mesenchymal markers in mesothelial cells. Omentum-derived mesothelial cells were treated with TGF-β1 at the concentrations shown. Epithelial markers: E-Cadherin, ZO-1, Occludin and Claudin-1; Mesenchymal markers: Fibronectin, Collagen I, Snail and α-SMA. **(A-B)** TGF-β1 concentration course. **(A)** Mesothelial markers. **(B)** Mesenchymal markers. Expression of all markers was analyzed by RT-qPCR and normalized to GAPDH expression. Data were analyzed by one-way ANOVA followed by post-hoc Holm-Sidak's test between treatments at each time point. Data represent the mean S.E.M. from three independent donor experiments. *$p < 0.05$; **$p < 0.01$; ***$p < 0.005$. **(C)** Phenotypic time-course changes of HPMCs in culture after TGF-β1 treatment. Omentum-derived mesothelial cells were treated for 0, 24, 48 and 72 h with TGF-β1 (1 ng/ml). (0 and 24 h) Characteristic epithelial morphology of polygonal shape cells from a confluent monolayer. (48 h) Loss of epithelial morphology and acquisition of fibroblast-like form. (72 h) Loss of epithelial morphology and acquisition of fibroblast-like phenotype with disruption of intercellular junctions characteristic of a migratory phenotype. One representative experiment of three is shown. Zeiss Axiovert 135 microscope. Magnification: 200x.

Supplemental Figure 2. TGF-β1 represses epithelial and induces mesenchymal markers in mesothelial cells in a time dependent manner. Omentum-derived mesothelial cells were treated with TGF-β1 for the time points shown. Epithelial markers: E-Cadherin, ZO-1, Occludin and Claudin-1; Mesenchymal markers: Fibronectin, Collagen I, Snail and α-SMA. **(A-H)** TGF-β1 time course. Control - white

bars, TGF-β1 (1ng/ml) - black bars. **(A)** E-Cadherin. **(B)** ZO-1. **(C)** Occludin 1. **(D)** Claudin-1. **(E)** Fibronectin. **(F)** Collagen I. **(G)** Snail. **(H)** α-SMA. Expression of all markers was analyzed by RT-qPCR and normalized to GAPDH expression. Data were analyzed by one- and two-way ANOVA followed by post-hoc Holm-Sidak's test between treatments at each time point. Data represent the mean S.E.M. from three independent donor experiments. *$p < 0.05$; **$p < 0.01$; ***$p < 0.005$; ****$p < 0.001$.

TGF-β1 down-regulated expression of epithelial markers E-cadherin, ZO-1, Occludin and Claudin-1 at 48 h (Figure S1A). This effect was TGF-β1-concentration dependent and showed a threshold for statistical significance at 1 ng/ml for E-cadherin and Occludin (Figure S1A). In addition, TGF-β1 up-regulated expression of mesenchymal markers Fibronectin, Collagen I, and α-SMA at 48 h (Figure S1B and S2 E-H). Snail expression did not vary in mesothelial cells incubated with different doses of TGF-β1 after 48 h of treatment (Figure S1B). Time-course experiments were then carried out to investigate temporal variation in TGF-β1 gene regulation. Down-regulation of epithelial markers was observed from 48 h onwards (Figure S1A and S2 A-D). The expression of epithelial markers ZO-1, Claudin and Occludin was affected by cell confluence and was most evident after 72 h of treatment (Figure S2 B-D). By contrast, mesenchymal markers were induced by 24 h, with Snail expression peaking at 2 h (Figure S2 E-H). Snail has been described to be involved in the alterations of intercellular adhesion during the MMT process, and its early activity here may contribute to the latter changes observed in epithelial markers (Figure S1A). Fibroblast-like architecture was visible after 48 h, and these changes were most evident after 72 h (Figure S2C). Phenotypic changes were not seen before 24 h (data not shown). In summary,

these results demonstrated that in primary HPMCs from multiple donors, 1 ng/ml of TGF-β1 induced changes consistent with an MMT process after 48 h.

Supplemental Figure 3. miRNA profiling in TGF-β1-stimulated HPMCs. Scatterplot of 2 technical replicates showing a significant correlation for all miRNA probes.

Supplemental Figure 4. miRNA profiling in TGF-β1-stimulated HPMCs and miRNA changes confirmation in *in vitro* and *ex vivo* models.. **(A)** miR-31 expression validation. Control - white bars, TGF-β1 (1ng/ml, 48 h) – black bars. **(B)** Relative expression of miR-31 in control omentum-derived mesothelial cells (HPMCs), TGF-β1 treated (1ng/ml, 48h) and cultured peritoneal effluent derived (PDE) cells with epithelial (E) and non-epithelial (NE) phenotype. Data represent the mean S.E.M. from five independent donor experiments. **(C)** Formalin-fixed paraffin embedded (FFPE) samples were manually macro-dissected to measure relative expression of miR-31 from a total of 44 patients. miR-31 expression is upregulated at the peritoneal membrane in peritoneal dialysis patients compared with uremic controls and is ns. Expression of miR-31 was analyzed by RT-qPCR and normalized to miR-191 expression. Data were analyzed by paired *t* test or one-way ANOVA followed by post-hoc Holm-Sidak's test comparing each condition mean with the control omentum-derived mean. *$p < 0.05$; ***$p < 0.005$.

Supplemental Figure 5. α-SMA expression is upregulated at the peritoneal membrane in peritoneal dialysis patients. Formalin-fixed paraffin embedded (FFPE) samples were stained for α-SMA. Upper panel, scale bar 300 μm; Lower panel, scale bar 80 μm.

Supplemental Figure 6. miR-21 3'UTR target site conservation for *PDZD2, S100A10, FGF-18*, *MATN2* and *PDCD4* across different animals. **(A-F, left panel)** Target sequences were acquired using TargetScan and alignment was performed with mega 6. Human complementary nucleotide sequences and 10 nucleotides up- and down-stream are presented. Conserved human complementary nucleotides at the seed binding area are displayed in red and whole nucleotide conservation is indicated with stars. **(A-F, right panel)** mRNA-miRNA hybrid was predicted using Diana v5.0. Seed binding area is displayed in red while remaining nearby nucleotides are shown in black (mRNA) and blue (miR-21). **(A-B)** *PDZD2*. **(C)** *S100A10*. **(D)** *FGF18*. **(E)** *MATN2.* **(F)** *PDCD4.*

Supplemental Figure 7. miR-31 expression in peritoneal dialysis effluent (PDE) from PD patients (n=230). RNA from 230 PDE samples was isolated and relative expression of miR-31 was normalized to miR-191 expression. Up-regulation of miR-31 expression in peritoneal dialysis effluent (PDE) from prevalent PD patients compared with incident cases. Data were analyzed by unpaired, Mann-Whitney test. Data represent the mean S.E.M. from samples. *****$p < 0.0005$.

Supplemental Figure 8. Scatter plot showing correlation of miR-21 and potential mRNA targets. **(A-N)** Relative mRNA expression in control omentum-derived mesothelial cells (HPMCs) – black circle, TGF-β1 treated (1ng/ml, 48h) – light grey and cultured peritoneal effluent derived (PDE) cells with epithelial (E) – dark grey and non-epithelial (NE) – pale grey, phenotype (n=5 for each group). **(A)** *NPPB*. **(B)** *PDZD2*. **(C)** *S100A10.* **(D)** *SASH1.* **(E)** *TIMP3.* **(F)** *AIM1L.* **(G)** *CASKIN1.* **(H)** *DUSP8.* **(I)** *FGF18.* **(J)** *MATN2.* **(K)** *NELL2.* **(L)** *RHOB.* **(M)** *SPRY1.* **(N)** *PDCD4.* Target mRNA gene expression was analyzed by RT-qPCR and normalized to GAPDH while miR-21 was normalized to miR-191.

Supplemental Figure 9. miR-21 target mRNA expression after miRNA mimic **(A, C, E, G, I, K)** or inhibitor **(B, D, F, H, J, L)** delivery in HPMCs **(A-L)** Target mRNA expression after 48h of miRNA mimic or inhibitor delivery (5 pM, 10 pM and 20 pM) in HPMCs. miR-control mimic and inhibitor – white bars, miR-21 mimic – black bars, miR-21 inhibitor – grey bars. **(A, B)** *SASH1*. **(C, D)** *AIM1L*. **(E, F)** *CASKIN1*. **(G, H)** *DUSP8.* **(I, J)** *NELL2*. **(K, L)** *SPRY1*. Target gene expression was analyzed by RT-qPCR and normalized to *GAPDH* expression respectively. Data were analyzed by matched factor two-way ANOVA followed by post-hoc Holm-Sidak's test. Data represent the mean S.E.M. from three (miRNA mimic) and six (miRNA inhibitor) independent donor experiments. *$p < 0.05$; **$p < 0.01$.

SUPPLEMENTAL FIGURE 1

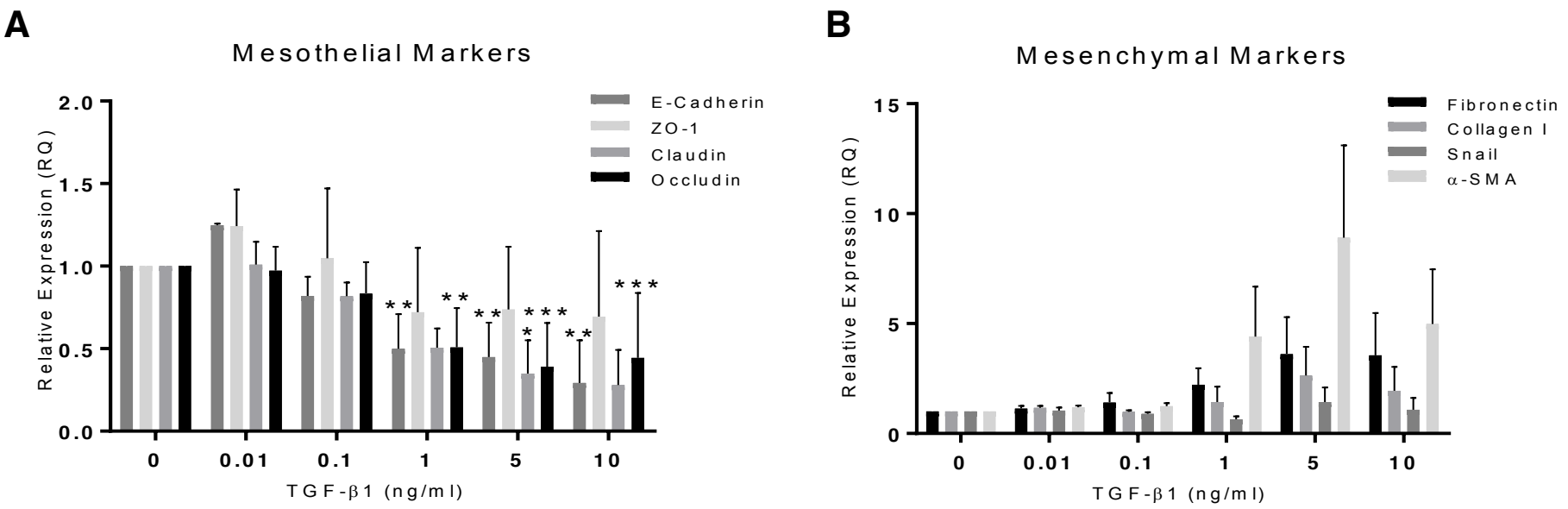

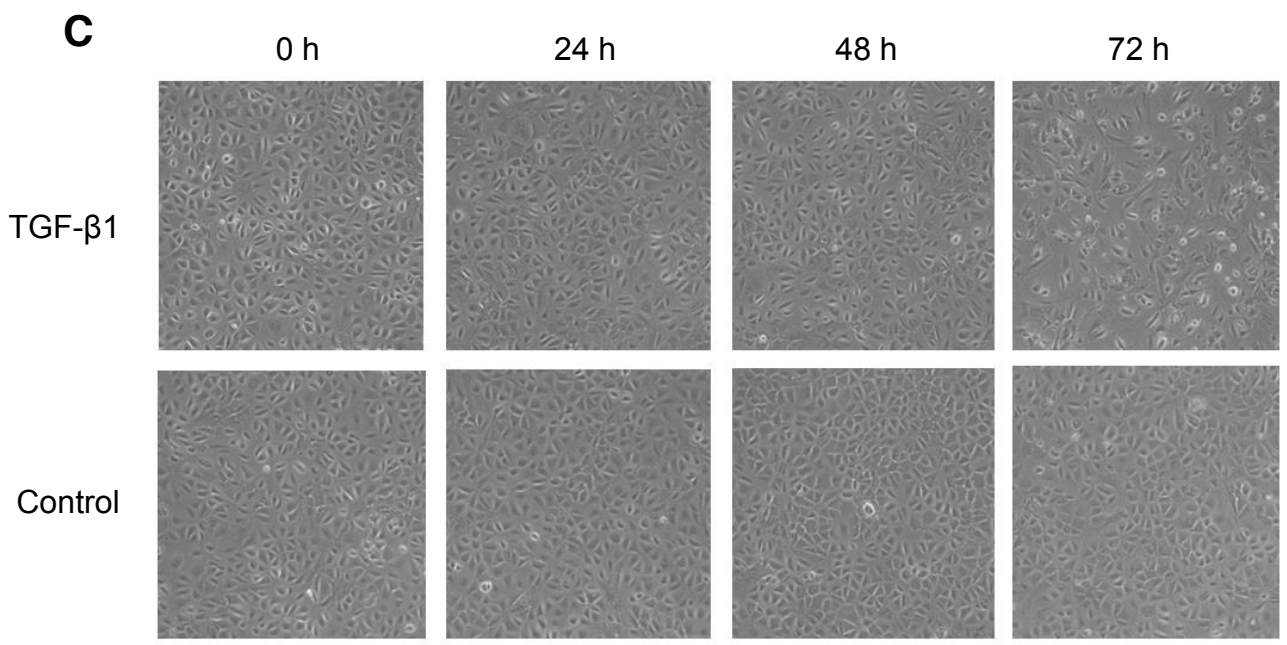

SUPPLEMENTAL FIGURE 2

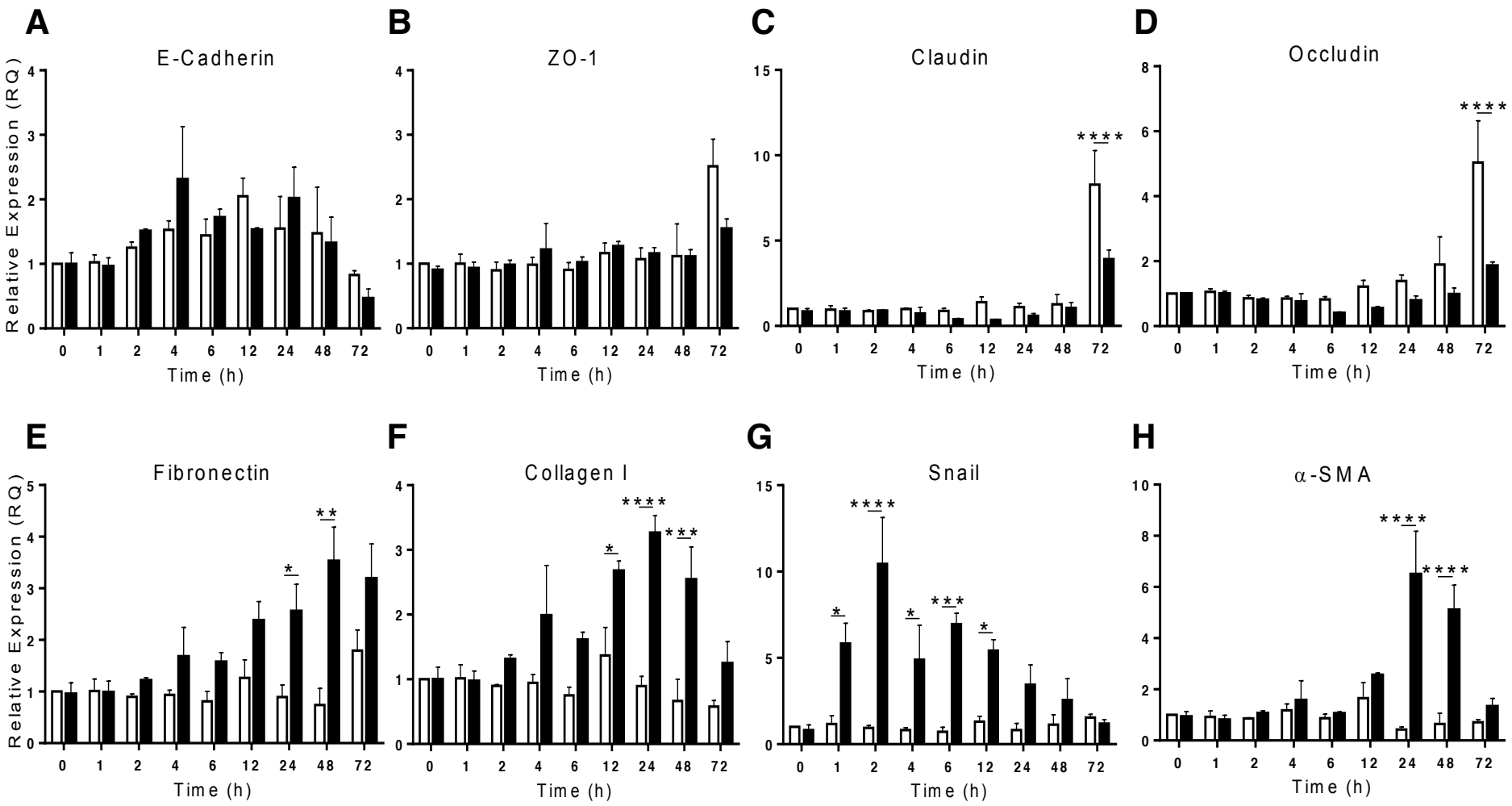

SUPPLEMENTAL FIGURE 3

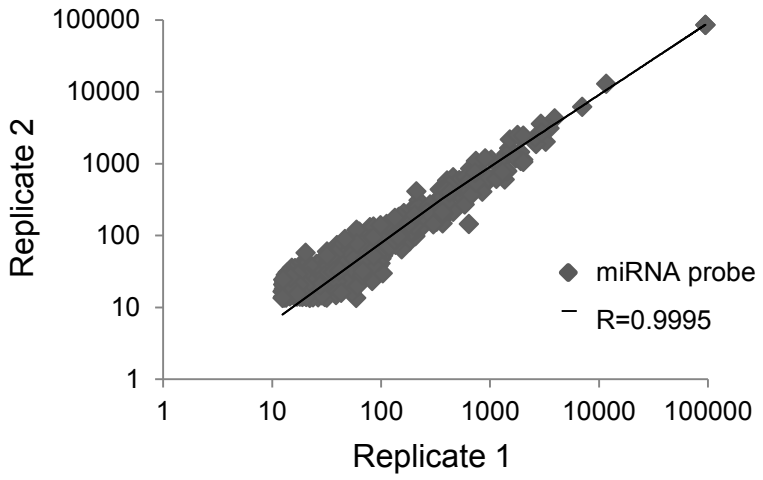

SUPPLEMENTAL FIGURE 4

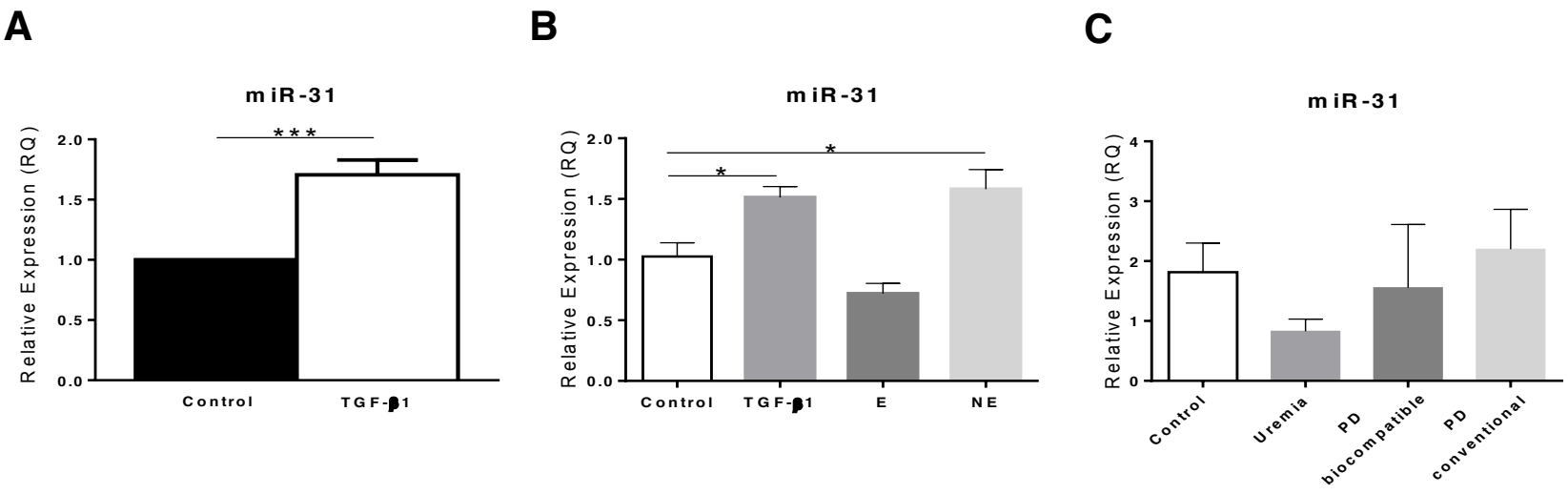

SUPPLEMENTAL FIGURE 5

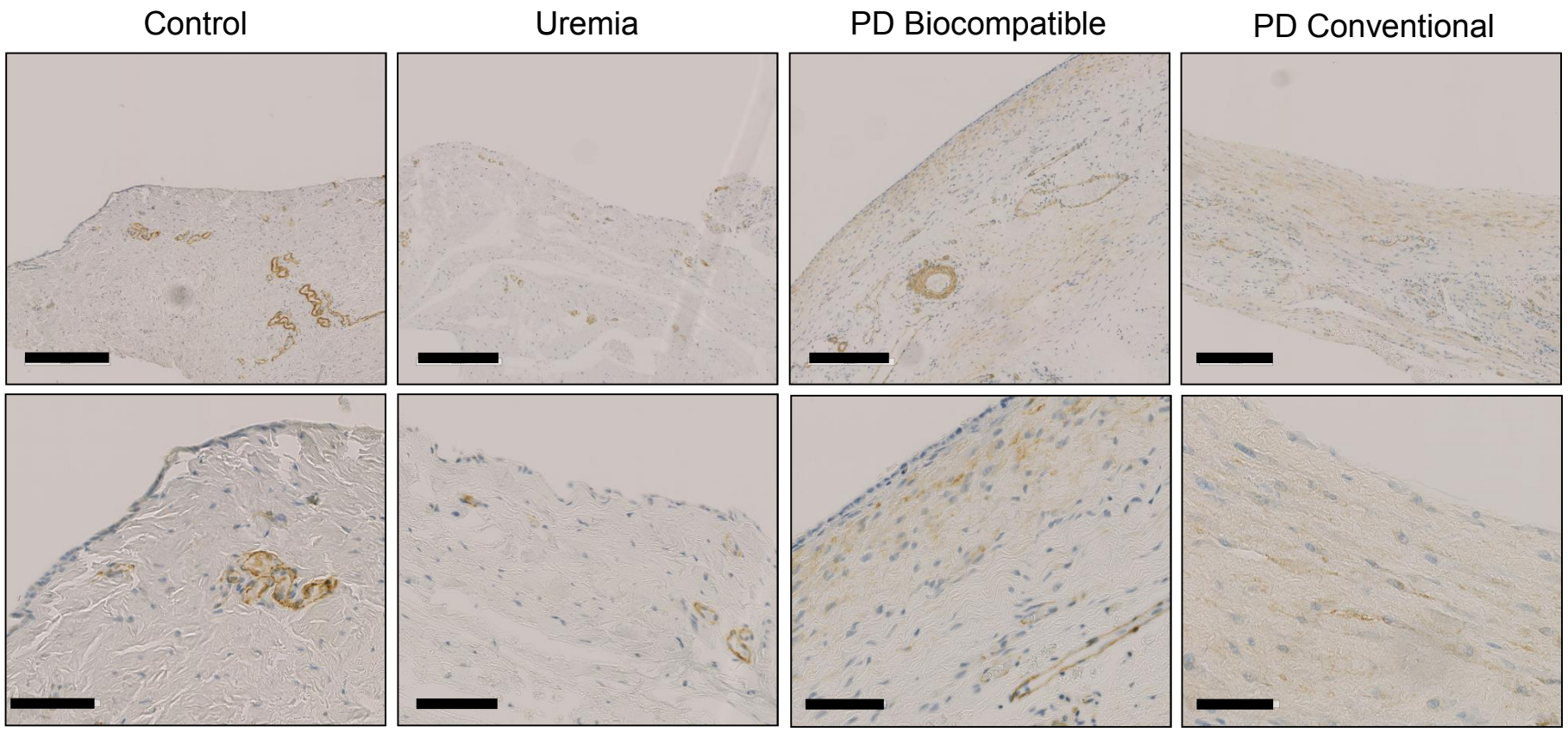

SUPPLEMENTAL FIGURE 6

A

```
           *                           **
Human      GAAUAGCACUUCUGAUAAGCUGUAUUAAAUA
Chimpanzee GAAUAGCACUUCUGAUAAGCUGUAUUAAACA
Rhesus     GAAUAGCACUUCUGAUAAACUGUAUUAAAUA
Rabbit     GAAUCG---------------AUGCUAAAUA
Mouse      GAGCGACAGUUCUGAUGAAUUGCAAUAAAUA
Rat        GAGCGACAGUUCUGACGAGUUGCAAUAAAUC
Cow        GGAAUGCAGUUUGGAUAAACUGUACUAAAUA
Horse      GAAAUGCAGUUCUGAUAAA-UGUAUGAAAUA
Dog        GAAAUGCAGUUCUGAGAAAGCAUACUAAAUA
Elephant   GGGUAGCAGCUCCACUGCUGUGCACUAAGCA
```

(*PDZD2*,Target Position 733-761)

```
5′ AA       U              3′
     UAGCA C  UCUGAUAAGCUG
     .|.|| |  ||||||||||.
     GUUGU G  AGACUAUUCGAU
3′   A     A UC             5′
```

B

```
                  * ** * **  *  *
Human      GUCAUUCACAAUAAGCUAUGAGGGUAAA
Chimpanzee GUCAUUCACAAUAAGCUAUGAGGGUAAA
Rhesus     GUCAUUCACAAUAAGCUAUGAGGGUAAA
Rabbit     GUCAUUUGCAGUGAGUUGUGAGGUCAAU
Mouse      GUCAUUCACAGUAAGCUAUGACGUAAGC
Rat        GUCACUCACAGUAAGCUAUGAGGUAAAA
Cow        GUCAUCCA--AUAAGCUAUGAUGGUAAU
Horse      GUCAUUCACGAUAAGCUAUGGGGGUAAA
Dog        GUCAUCCACAAUAAGCUAUGAGGGUAAA
Elephant   ----UUCACAAUAAGCUAUGAGGGUAAA
```

(*PDZD2*,Target Position 2436-2464)

```
5′       UG        AUUCACA          3′
   UUAAC  GUCAGUC        AUAAGCUA
   |.|||  .||||||        ||||||||
   AGUUG  UAGUCAG        UAUUCGAU
3′                AC               5′
```

C

```
                 * **  *****  *  ****
Human      -------CCAGAUAAGCUUUUGAUUUUU
Chimpanzee -------CCAGAUAAGCUUUUGAUUUUU
Rhesus     -------CCAGAUAAGCUUUUGAUUUUU
Rabbit     AAU---GCCAGAUAAGCUUCUGAGUUUU
Mouse      AAU---GGCAGAGAAGCUUCUGAGUUUU
Rat        AAU---GACAGAGGAGCUUUCGAGUUUU
Cow        AAG----CCAGAUAAGCUUUUGAUUUUU
Horse      AAG----CCGGAUAAGCUUUUGAUUUUU
Dog        AAGAAAGCCAGAUAAGCUUUUGAUUUUU
Elephant   AAU---GCCAGAUAAGCUUUUGGUUUUU
```

(*S100A10*,Target Position 156-184)

```
5′ UA    C              U 3′
     AAUA CA    GAUAAGCU
     ||.| ||    ||||||||
     UUGU GU    CUAUUCGA
3′   G    A  CAGA        U 5′
```

D

```
           ********  ******************
Human      UUAUAUAUAUAUAAGCUAUUUAUUUCAC
Chimpanzee UUAUAUAUAUAUAAGCUAUUUAUUUCAC
Rhesus     UUAUAUAUAUAUAAGCUAUUUAUUUCAC
Rabbit     UUAUAUAUAUAUAAGCUAUUUAUUUCAC
Mouse      UUAUAUAU--AUAAGCUAUUUAUUUCAC
Rat        UUAUAUAU--AUAAGCUAUUUAUUUCAC
Cow        UUAUAUAUAUAUAAGCUAUUUAUUUCAC
Horse      UUAUAUAUAUAUAAGCUAUUUAUUUCAC
Dog        UUAUAUAUAUAUAAGCUAUUUAUUUCAC
Elephant   UUAUAUAUAUAUAAGCUAUUUAUUUCAC
```

(*FGF-18*,Target Position 701-729)

```
5′ AU       UAUAUAU          3′
     AUAUUA        AUAAGCUA
     |.||.|        ||||||||
     UGUAGU        UAUUCGAU
3′   U       CAGAC           5′
```

E

```
                    ***** **   **
Human      GUGAGAAUGAAUAAGCUAUGCAAGGUA-
Chimpanzee GUGAGAAUGAAUAAGCUAUGCAAGGUA-
Rhesus     GUGAGAAUGAAUAAGCUAUGCAAGGCA-
Rabbit     GGGAGAGUAAAUAAGCUAUACAAGGCG-
Mouse      -UGAGAAUAAAUAAGCUGCGCAGUGUAG
Rat        --------GAAUAAGCUGUGCAGGG---
Cow        GUGAGAACAAAUAAGCUAUGCAAGAUA-
Horse      GUGAGAACAAAUAAACUAUGCAAGAUA-
Dog        GUGAGAACAAAUAAGCUAUGCAAAAUA-
Elephant   GUGAGAAUAAAUAAGCUAUGCAAGGUA-
```

(*MATN2*,Target Position 214-242)

```
5′ UA C G  G  AA  A          3′
     C A GU AG  UG AUAAGCUA
     | | .| ||  || ||||||||
     G U UA UC  AC UAUUCGAU
3′   A U G  G  AG            5′
```

F

```
           *  * **   ********* **   **
Human      GAAUAUUCUAAUAAGCUACCUUUUGUAA
Chimpanzee GAAUAUUCUAAUAAGCUACCUUUUGUAA
Rhesus     GAAUAUUCUAAUAAGCUACCUUUUGUAA
Rabbit     GAAUAUUCCAAUAAGCUACCUUUUGUAA
Mouse      GG-UGUUCUGAUAAGCUACUUUC--UAA
Rat        GGGUGUUCUGAUAAGCUACUUUC--UAA
Cow        GGAUAUUCUCAUAAGCUACCUUUUGUAA
Horse      GAAUAUUCUCAUAAGCUACCUUUUGUAA
Dog        GAAUAUUCUCAUAAGCUACCUUUUGUAA
Elephant   GAAUAUUAUAAUAAGCUACCUUUUGUAA
```

(*PDCD4*,Targe t Position 220-248)

```
5‘  G           A        3'
     AAUAU   UCU AUAAGCUA
     ||.||   ||| ||||||||
     UUGUA   AGA UAUUCGAU
3‘ AG     GUC   C        5'
```

SUPPLEMENTAL FIGURE 7

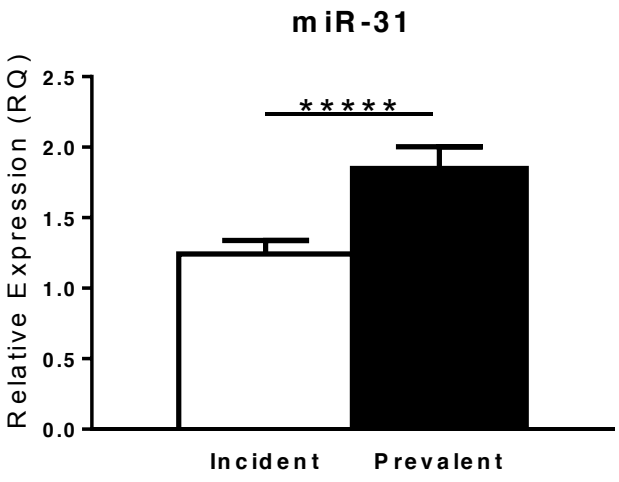

SUPPLEMENTAL FIGURE 8

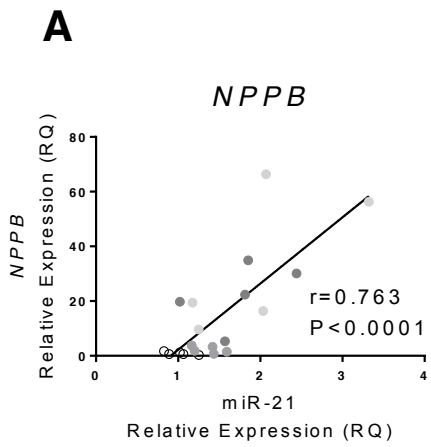

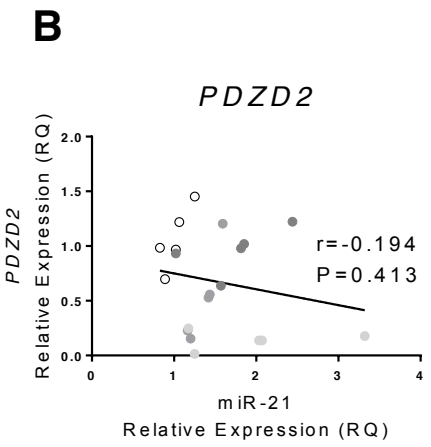

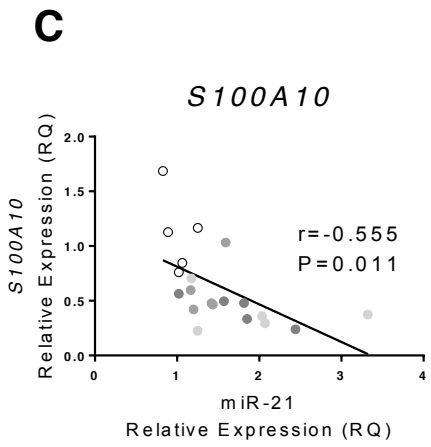

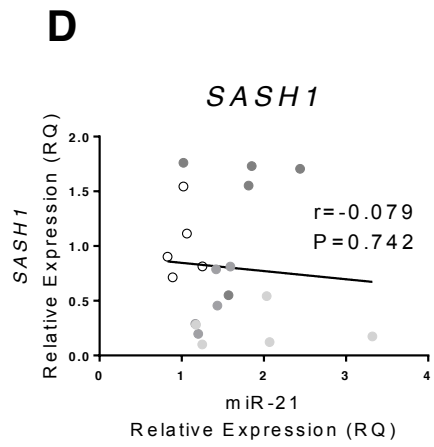

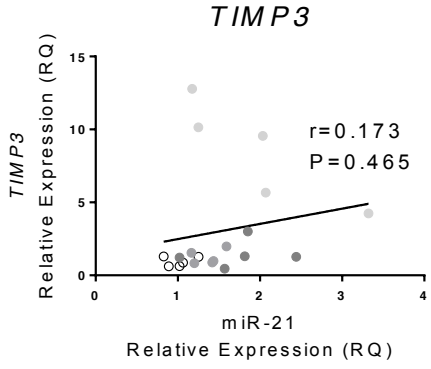

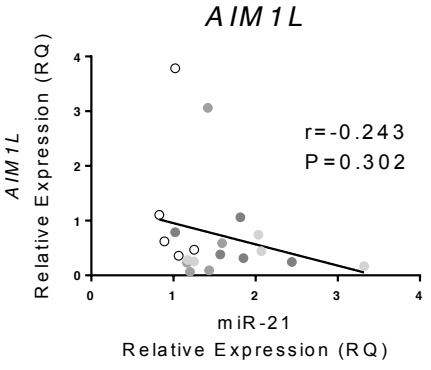

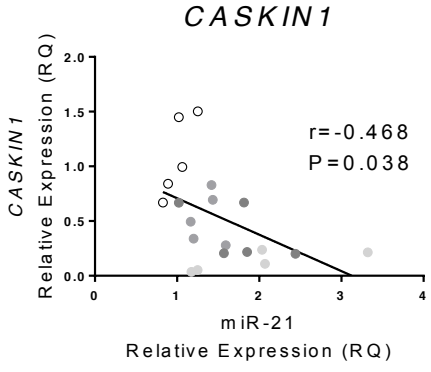

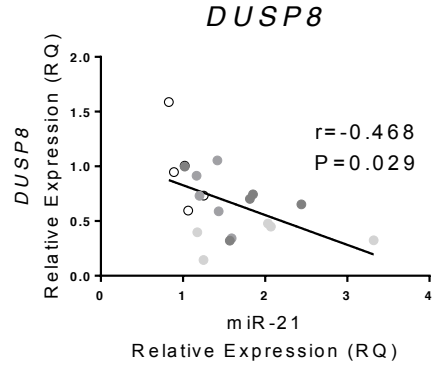

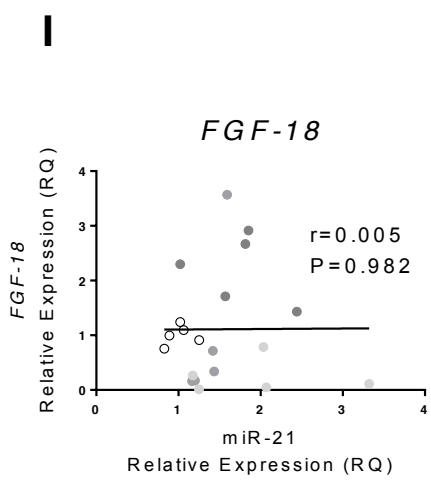

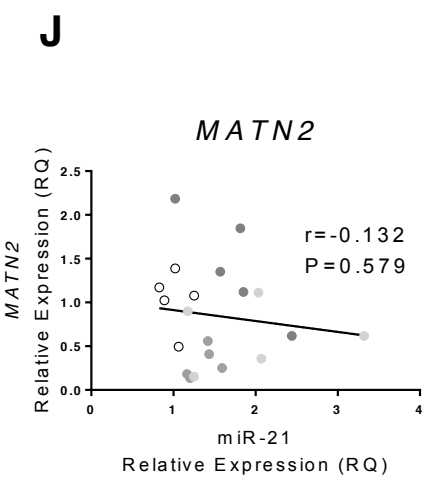

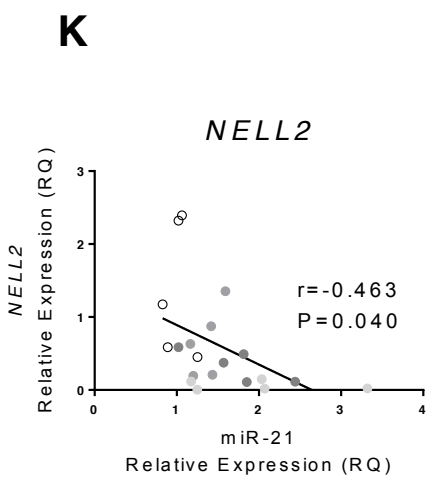

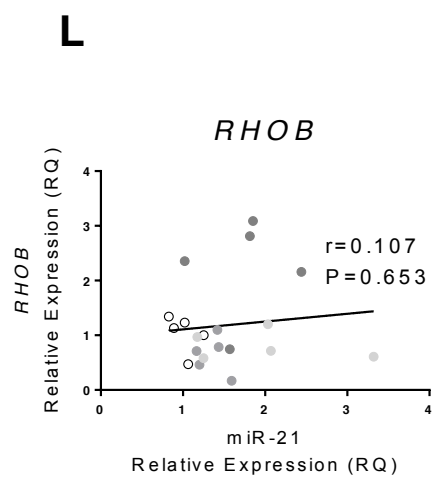

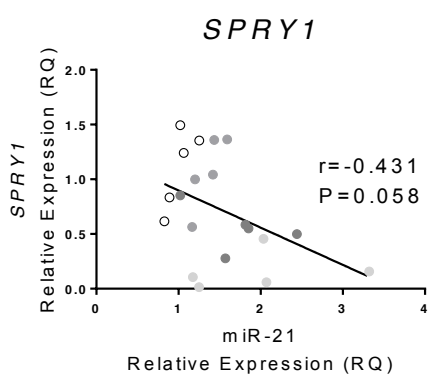

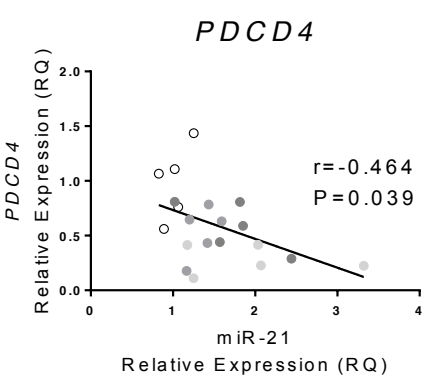

SUPPLEMENTAL FIGURE 9

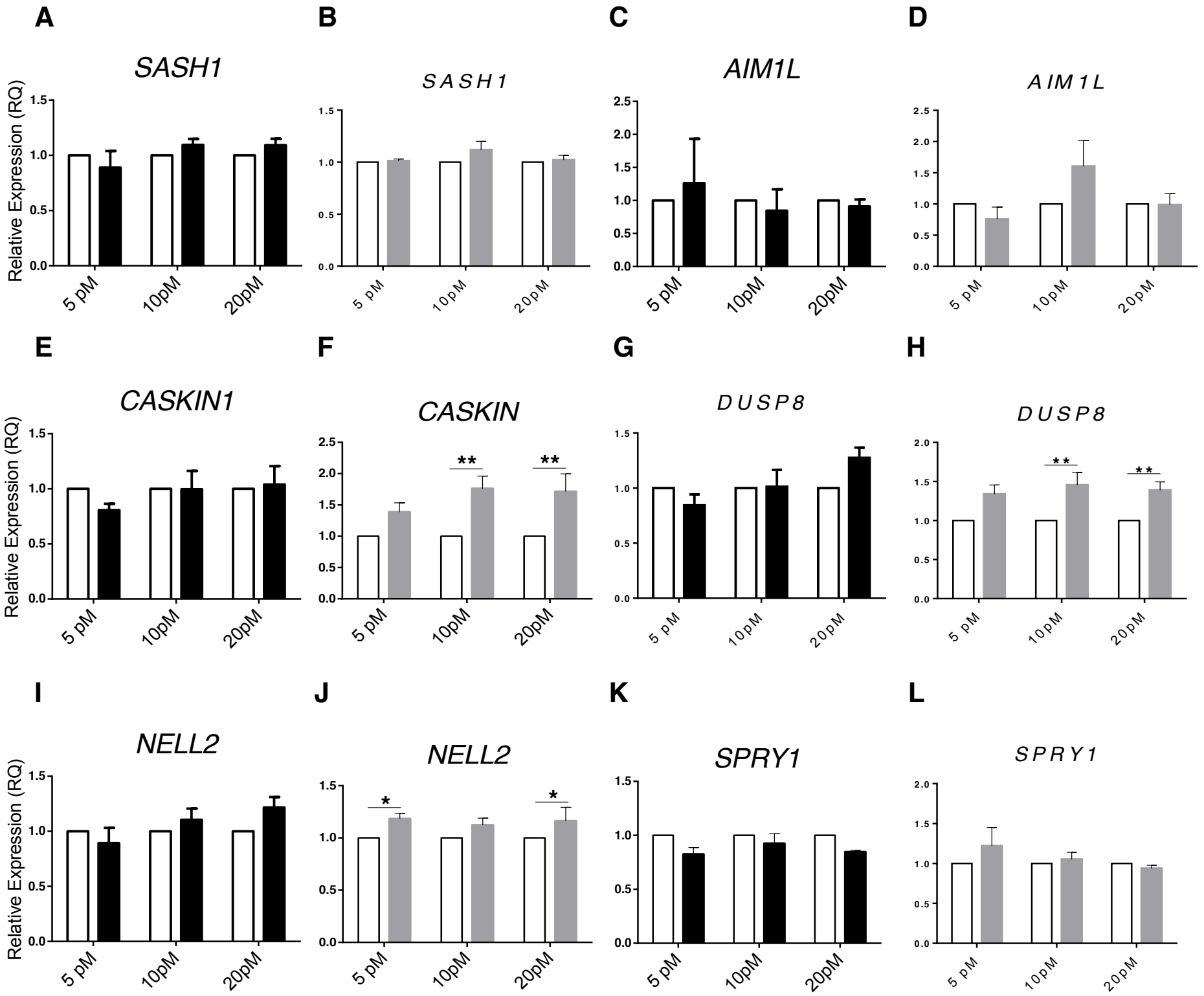

Characteristic	Patients (n=230)
Age (yr)	54.3±16.2
Body mass index (kg/m^2)	26.5±5.3
Average Dialysate glucose concentration (%)	1.56±0.38
4-hour D/P creatinine	0.75±0.15
Duration of PD (month)	2.85 (1.23, 16.19)
Albumin (g/L)	34.9±4.9
Dialysate IL-6 (pg/mL)	3.57 (0.94, 10.44)
Dialysate IFN-γ (pg/mL)	0.97 (0, 4.49)
Dialysate IL-1β (pg/mL)	0 (0, 0.072)
Dialysate TNF-α (pg/mL)	0 (0, 0.20)
Plasma IL-6 (pg/mL)	1.25 (0.67, 2.49)
Urine volume (mL)	904 (292, 1595)
Comorbidity score	1 (0, 1)
Icodextrin use (%)	36.30
Biocompatible solution use (%)	7.30
Men (%)	54.30
APD use (%)	31.20
Peritonitis count	0 (0, 0)

Supplemental Table 1. Study population descriptive characteristics. Data are presented as the mean ± SD, median (interquartile range), or as percentage.

Variable	miR-31	miR-21
miR-21	0.26***	
Age	0.05	0.03
Body mass index	0.16*	0.15*
Dialysate glucose concentration	0.22**	0.04
4-hour D/P creatinine	0.13	0.16*
Duration of PD	0.19**	0.13*
Albumin	0.03	-0.10
Dialysate IL-6	0.04	0.28***
Dialysate IFN-γ	0.09	-0.10
Dialysate IL-1β	0.00	0.006
Dialysate TNF-α	0.05	0.04
Plasma IL-6	0.00	0.11
Urine volume	-0.24***	-0.19**
Comorbidity	0.03	0.02
Icodextrin use	0.00	0.28***
Biocompatible solution use	0.08	0.10
Gender	0.09	-0.02
Type of PD	0.06	-0.10
Peritonitis count	0.18**	0.25***

Supplemental Table 2. PDE miR-21 correlation with clinically important parameters. * $p<0.05$, ** $p<0.01$, *** $p<0.001$

Variable	Coefficient (95% Confidence Interval)	p value
Peritonitis Count	0.052 (0.006, 0.098)	0.028
miR-21	0.087 (0.038, 0.136)	0.001
Biocompatible solution usage	0.18 (-0.04, 0.40)	0.114
Plasma Albumin	0.0096 (-0.001, 0.020)	0.077
Urine volume	-0.00010 (-0.00017, -0.00003)	0.003
Use of CAPD vs APD	0.14 (0.02, 0.25)	0.023

Supplemental Table 3. Multivariable Regression of miR-31. To understand the relevance of all parameters included in Supplemental Table 2 for the described up-regulation of miR-31, multivariable linear regression with backwards stepwise variable selection was performed. Stepwise variable selection determined a group of tighter risk factors that associated with miR-31 in predicting PD outcome that are detailed at the table above. Results for dialysate cytokines and mir-31 are given per log order. (n=230).